Studies on Novel Anisotropic Polymer Composites Synthesized from Mesomorphic Colloidal Suspensions of Cellulose Nanocrystals

2015

Mio TATSUMI

Contents

List of Abbreviations

CNC	Cellulose nanocrystal
DMA	Dynamic mechanical analysis
DSC	Differential scanning calorimertry
E'	Dynamic storage modulus
E''	Dynamic loss modulus
FE-SEM	Field emission scanning electron microscope
FT-IR	Fourier transform infrared spectroscopy
HEMA	Hydroxyethyl methacrylate
HMPPh	2-hydroxy-2-methylpropiophenone
HPC	Hydroxypropyl cellulose
IPN	Interpenetrating polymer network
MF	Magnetic field
PE	Polyethylene
PEG	Polyethylene glycol
PHEMA	Poly(2-hydroxyethyl methacrylate)
POM	Polarized optical microscope
SD	Shear direction
Tanδ	Loss tangent (= E''/E')
TD	Transverse direction
TEM	Transmission electron microscopy
T_g	Glass transition temperature
WAXD	Wide-angle X-ray diffraction

Chapter 1

General Introduction

Cellulose nanocrystals (CNCs), or cellulose nanocrystallites as synonym, are fragmented microfibrils of fibrous celluloses. They are crystalline rod-like particles and conventionally obtained by hydrolysis of native cellulose fibers (e.g. cotton and wood pulp) with sulfuric acid.[1,2] The sizes of CNCs (esp., the longitudinal dimensions) are thought to correlate with the level-off degree of polymerization of the constituent cellulose molecules; for example, cotton-derived CNCs have ~100 nm lengths and ~5 nm widths. In the case where sulfuric acid is used as the agent for hydrolyzing native celluloses, the surfaces of the resulting CNCs are sulfated and negatively charged. In water, therefore, the CNC particles show an adequate dispersibility to give a stable colloidal suspension. Above a critical CNC concentration, typically to 3–5 wt % for the cotton-derived CNCs, the visually homogeneous suspension phase-separates into an isotropic upper phase and an anisotropic lower one in the course of quiescent standing of the fluid sample. This phenomenon is ascribable to the self-assembling character of rigid CNCs to form a liquid crystal, and the observed anisotropic mesophase (lower phase) is usually of a chiral nematic type.[1]

CNCs would be additives or fillers offering not only ″optical functionality″ derived from the mesomorphic characteristics but also ″mechanical high-performance″ to polymer matrices, the latter action being based on the nanoscale dimension of high aspect ratio and the inherent high stiffness. Actually, there have been considerable efforts to acquire high-performance polymer solid materials containing CNCs.[3–5] In many of the examples, CNCs were compounded with thermoplastic polymers by simple mechanical mixing.[6–9] Attempts to fabricate CNC aggregates showing mesomorphy have also been made, and chiral-nematically ordered films of CNCs were prepared by casting from CNC suspensions in water or other solvents.[1,10,11]

Meanwhile, with regard to the synthesis of cellulose-based unique microcomposites, Nishio and Miyashita et al. formerly developed a chemical blending technique of *solution coagulation*/*bulk polymerization*.[12–15] An essential part of the method is *in situ* polymerization of a vinyl monomer as coagulant and/or impregnant used to form cellulose gels, enabling us to obtain an interpenetrating network (IPN) consisting of cellulose/synthetic

polymer. Using a similar method, Nishio et al. have also succeeded in preserving a chiral nematic mesophase of hydroxypropyl cellulose (HPC) in polymer composites.[12,13,16] In view of the successful examples of cellulosic molecular composites, it may also be possible to immobilize the mesomorphic order of CNC suspensions in polymer solids and gels. Such a locking-in method can be of great significance in design and fabrication of new polymeric materials exploiting the CNCs' potential in optical and mechanical performances.

In conditioning of the optical, mechanical, or thermomechanical properties of CNC-containing materials, the orientation control of CNCs is also of great importance. There were various attempts to align CNCs in aqueous media and fix the orientation state in the dried films or polymer composites, for the purpose of making their properties anisotropic and upgraded. For example, CNCs were aligned in the suspensions by deformation of shearing[17] or drawing,[18–20] and also by a non-contact technique of applying magnetic fields.[21–23]

In accord with the backgrounds stated above, the author would like to exemplify possible routes leading to novel anisotropic polymer materials, in which some ordered arrangement of the mesomorphic CNC assembly is perpetuated to reinforce the matrix polymer and to bring specific properties to the whole bulk as well. The approach and ensuing results are expected to greatly contribute to further development of the availability of CNCs as fillers.

Outline of this thesis

This thesis entitled “Studies on Novel Anisotropic Polymer Composites Synthesized from Mesomorphic Colloidal Suspensions of Cellulose Nanocrystals” consists of five chapters. The main purpose of this thesis is to enhance the availability of CNCs toward the new development of modern compositional materials of cellulose and polymers. The result of the studies will be a useful example demonstrating the capability of CNC as fillers. The outline of the present thesis is described below and also illustrated schematically in Figure 1-1.

In chapter 1, after introducing CNCs and the current situation of scientific research about them, the significance of advanced utilization of CNCs as fillers was explained. The outline of this thesis is also summarized briefly.

In chapter 2, an attempt was made to synthesize novel composites comprising

poly(2-hydroxyethyl methacrylate) (PHEMA) and CNC (derived from cotton cellulose) from suspensions of CNC in an aqueous 2-hydroxyethyl methacrylate (HEMA) monomer solution. By way of polymerization of HEMA in different phase situations of the suspensions, the authors obtained films of three polymer composites, PHEMA-CNC_{iso}, PHEMA-CNC_{aniso}, and PHEMA-CNC_{mix}, coming from the isotropic phase, anisotropic phase, and embryonic non-separating mixture, respectively. All the composites were transparent and, more or less, birefringent under a polarized optical microscope (POM). A fingerprint texture typical of chiral nematic (cholesteric) liquid crystals of longer pitch spread widely in PHEMA-CNC_{aniso} but rather locally appeared in PHEMA-CNC_{iso}. It was shown by differential scanning calorimetry (DSC) and a tensile test that any of the CNC incorporations into the PHEMA matrix improved the original thermal and mechanical properties of this amorphous polymer material. In dynamic mechanical analysis (DMA), the locking-in of the respective CNC assemblies gave rise to an increase in the glass-state modulus E' of PHEMA as well as a marked suppression of the E'-falling at temperatures higher than T_g (~110 °C) of the vinyl polymer. It was also observed for the composites that their modulus E' rerose in a range of ca. 150–190 °C, which was attributable to a secondary cross-linking formation between PHEMA chains mediated by the acidic CNC filler. The mechanical reinforcement effect of the CNC dispersions was ensured in the tensile measurement, whereby PHEMA-CNC_{aniso} was found to surpass the other two composites in stiffness and strength.

In chapter 3, polymer composites reinforced with an oriented CNC assembly were prepared from suspensions of CNC in aqueous HEMA via magnetic field application to the suspensions followed by polymerization treatment. A static or rotational magnetic field was applied to the isolated isotropic and anisotropic phases of the CNC suspensions phase-separated after quiescent standing. UV-induced polymerization of the monomer perpetuated the respective states of magnetic orientation invested for the CNC dispersions, to yield variously oriented CNC/PHEMA composites. The structural characterization was carried out by use of X-ray diffractometry and optical and scanning electron microscopy. The result indicated that CNCs were aligned in the composites distinctively according to the static or rotational magnetic application when the anisotropic phases were used, whereas such a specific CNC orientation was not appreciable when the isotropic phases were sampled. This marks out effectiveness of a coherent response of CNCs in the mesomorphic assembly. In DMA experiments in tensile or compressive mode, we observed a clear mechanical

anisotropy for the polymer composites synthesized from wholly anisotropic suspensions under static or rotational magnetization. The higher modulus (in compression) was detected for a composite reinforced by locking-in the uniaxial CNC alignment attainable through conversion of the initial chiral nematic phase into a nematic phase in the rotational magnetic field.

In chapter 4, the authors turned attention to preparing oriented films from aqueous suspensions of CNC by a shearing method. Rotating glass vials each containing a CNC/water suspension under evaporation resulted in formation of translucent films of CNC *per se*. Structural characterization of the dry films was carried out by use of X-ray diffractometry and optical and scanning electron microscopy. The orientation pattern of CNCs in the films was much affected by pH condition of the starting suspensions; that is, the longitudinal axes of CNCs aligned preferentially perpendicular to the shear direction (SD) in the acidic condition of pH = 2.0, while an ordinary orientation of CNCs aligning parallel to SD was observed in the neutral condition of pH = 6.7 (adjusted with NaOH addition to the acidic suspension, however). To interpret the two distinct orientation patterns, first, it was inspected whether a mesomorphic ordered phase arrived or not in the two sheared and dried suspensions, different from each other in the counterions of surface-sulfated CNCs. As to the orientation development from the suspension of pH = 2, it was particularly assumed that the arising nematic planar domains would have been rolled up into a transversely extended body with the director perpendicular to SD. For the two film preparations, the orientation parameter of the longitudinal axis of CNC was quantified by WAXD intensity measurements, and the data were compared with those for other CNC-oriented materials such as CNC/polymer composites synthesized by immobilizing CNC suspensions via magnetic field application.

In chapter 5, major results obtained through this series of studies using CNCs are summarized.

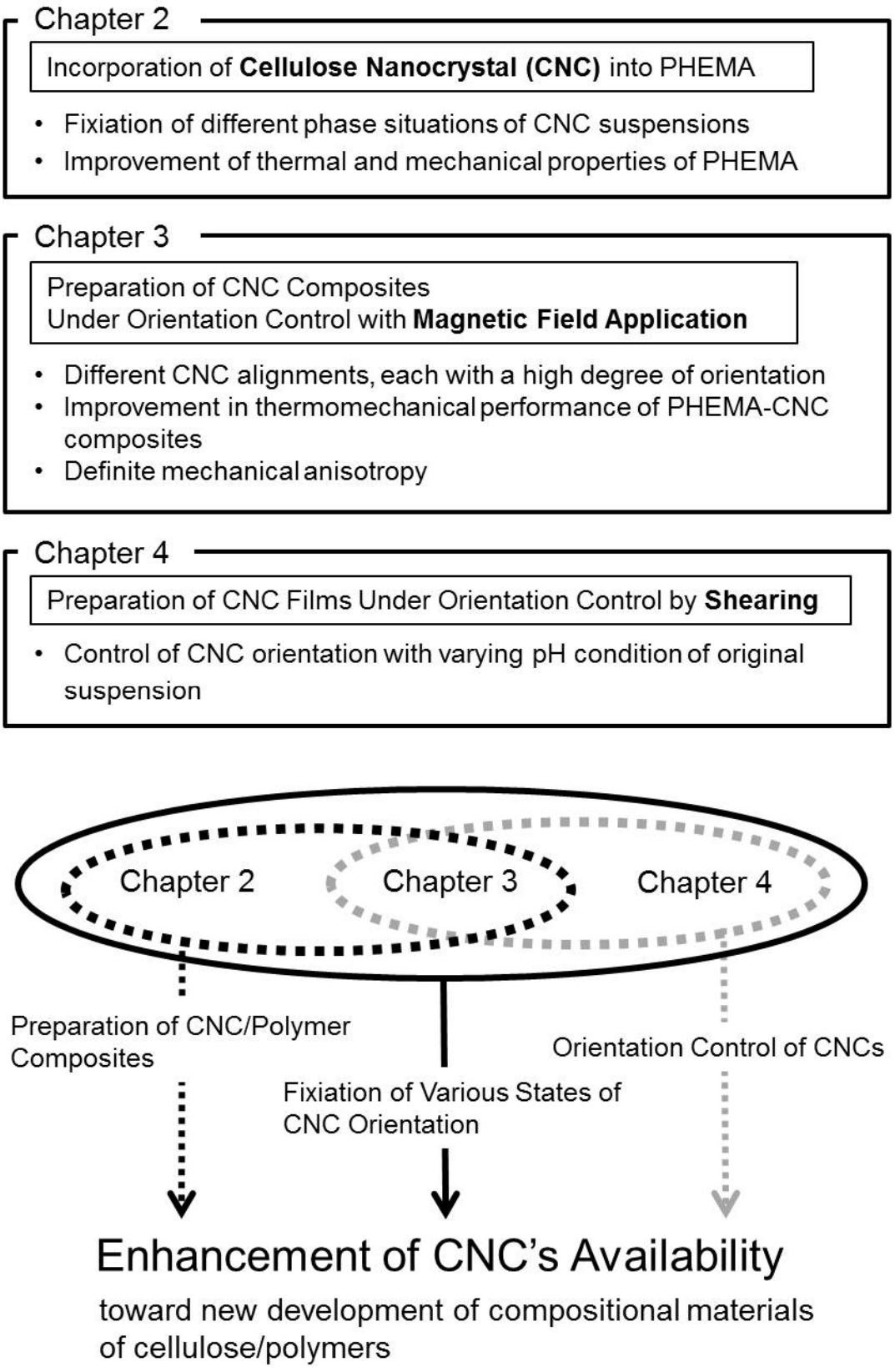

Figure 1-1. Schematic representation of the outline of this thesis.

References

(1) Revol, J. -F.; Bradford, H.; Giasson, J.; Marchessault, R. H.; Gray, D. G. *Int. J. Biol. Macromol.* **1992**, *14*, 170–172.

(2) Guo, J. -X.; Gray, D. G. Chapter 2. In *Cellulosic Polymers, Blends and Composites;* Gilbert, R. D., Ed.; Hanser: Munich/New York, 1994.

(3) Habibi, Y.; Lucia, L. A.; Rojas, O. J. *Chem. Rev.* **2010**, *110*, 3479–3500.

(4) Klemm, D.; Kramer, F.; Moritz, S.; Lindström, T.; Ankerfors, M.; Gray, D. G.; Dorris, A. *Angew. Chem. Int. Ed.* **2011**, *50*, 5438–5466.

(5) Moon, R. J.; Martini, A.; Nairn, J.; Simonsen, J.; Youngblood, J. *Chem. Soc. Rev.* **2011**, *40*, 3941–3994.

(6) Favier, V.; Chanzy, H.; Cavaillé, J. Y. *Macromolecules* **1995**, *28*, 6365–6367.

(7) Azizi Samir, M. A. S.; Alloin, F.; Sanchez, J. -Y.; El Kissi, N.; Dufresne, A. *Macromolecules* **2004**, *37*, 1386–1393.

(8) Petersson, L.; Kvien, I.; Oksman, K. *Compo. Sci. Tech.* **2007**, *67*, 2535–2544.

(9) Li, Q.; Zhou, J.; Zhang, L. *J. Polym. Sci., Part B: Polym. Phys.* **2009**, *47*, 1069–1077.

(10) Revol, J. -F.; Godbout, L.; Gray, D. G. *J. Pulp Pap. Sci.* **1998**, *24*, 146–149.

(11) Viet, D.; Beck-Candanedo, S.; Gray, D. G. *Cellulose* **2007**, *14*, 109–113.

(12) Nishio, Y. Chapter 5. In *Cellulosic Polymers, Blends and Composites;* Gilbert, R. D., Ed.; Hanser: Munich/New York, 1994.

(13) Nishio, Y. *Adv. Polym. Sci.* **2006**, *205*, 97–151.

(14) Nishio, Y.; Hirose, N. *Polymer* **1992**, *33*, 1519–1524.

(15) Miyashita, Y.; Kimura, N.; Nishio, Y.; Suzuki, H. *Kobunshi Ronbunshu* **1994**, *51*, 466–471.

(16) Nishio, Y.; Yamane, T.; Takahashi, T. *J. Polym. Sci. Polym. Phys. Ed.* **1985**, *23*, 1043–1052.

(17) Nishiyama, Y.; Kuga, S.; Wada, M.; Okano, T. *Macromolecules* **1997**, *30*, 6395–6397.

(18) Ureña-Benavides, E. E.; Brown, P. J.; Kitchens, C. L. *Langmuir* **2010**, *26*, 14263–14270.

(19) Uddin, A. J.; Araki, J.; Gotoh, Y. *Biomacromolecules* **2011**, *12*, 617–624.

(20) Gindle, W.; Keckes, J. *J. Appl. Polym. Sci.,* **2007**, *103*, 2703–2708.

(21) Kimura, F.; Kimura, T.; Tamura, M.; Hirai, A.; Ikuno, M.; Horii, F. *Langmuir* **2005**, *21*,

2034–2037.

(22) Kvien, I.; Oksman, K. *Appl. Phys. A: Mater. Sci. Process.* **2007**, *87*, 641–643.

(23) Pullawan, T.; Wilkinson, A. N.; Eichhorn, S. J. *Biomacromolecules* **2012**, *13*, 2528–2536.

Chapter 2

Polymer Composites Reinforced by Locking-In a Liquid-Crystalline Assembly of Cellulose Nanocrystals

2.1. Introduction

Acid hydrolysis of native cellulose fibers yields a highly crystalline rod-like particle, cellulose nanocrystal (CNC).[1,2] Conventionally this treatment is made with sulfuric acid, so that the surface of CNC is sulfated. In water, therefore, the CNC particles are each negatively charged and show an adequate dispersibility to assume a stable colloidal suspension. With a relatively small increase in the CNC concentration, however, the aqueous suspension manifests a unique character to form a self-ordering structure by spontaneous phase separation; that is, above a critical concentration of several wt % CNC, the visually homogeneous suspension phase-separates into an isotropic upper phase and an anisotropic lower one in the course of quiescent standing.[1] The anisotropic phase is birefringent and exhibits a fingerprint pattern under a polarized optical microscope, indicating a cholesteric (or chiral nematic) arrangement of the CNC rods in the mesophase.[1–3]

From a practical standpoint, a number of approaches have been conducted to design and fabricate high-performance nanocomposites based on CNCs.[4–7] In many cases, CNCs were compounded with thermoplastic polymers by simple mechanical mixing. For example, CNC (from tunicate)/water suspensions were homogeneously mixed with a latex of poly(styrene-*co*-butyl acrylate) ($T_g \approx 0$ °C) and air-dried to obtain composite films.[4] It was reported there that the modulus G' in shear oscillation was enhanced by more than two orders of magnitude in the rubbery state at $T > T_g$ of the copolymer matrix, even when the CNC filler was loaded at quite a low concentration of 6 wt %.

Meanwhile, some researchers have made an attempt to solidify the mesophase structure appearing in CNC/water suspensions, in relation to new designing of optically functional materials. Revol et al. obtained CNC-aggregate films retaining a chiral nematic order by simple evaporation of water from the aqueous suspensions.[1,8] The chiral nematic pitch of the resulting films were controlled by changing the ionic strength of the casting suspensions,

e.g., by addition of conventional salts, so that the film products (or papers) imparted various colorations due to selective light reflection.[8] Viet et al. also prepared birefringent films by casting from CNC suspensions in a polar aprotic solvent such as dimethyl sulfoxide.[9] In a pretreatment for the preparation, first CNC/water suspensions were freeze-dried, and then the CNC residues were sonicated in the polar organic solvent selected.

In this chapter, the authors show another possible route leading to a novel polymeric material perpetuating the mesophase arrangement of CNC therein. Namely, CNC particles are mixed with an aqueous solution of a vinyl monomer, 2-hydroxyethyl methacrylate (HEMA), containing a radical initiator, so as to form a suspension showing the optically biphasic separation above a certain concentration. In the successful phase-separation, for instance, polymerizing the monomer for the lower-situated anisotropic phase would preserve the initial ordered assembly of CNC into the resulting poly(2-hydroxyethyl methacrylate) (PHEMA) matrix. This preparation method is substantially based on a chemical blending technique of "solution coagulation/bulk polymerization" reported formerly by Nishio and Miyashita et al.[10–12] to obtain an interpenetrating network (IPN) consisting of cellulose/synthetic polymer. In one of those studies, cellulose/PHEMA composites were prepared from cellulose solutions in *N,N*-dimethyl acetamide/LiCl by coagulation with HEMA and subsequent polymerization of the monomer as an impregnant to form cellulose gels.[10]

In addition to perpetuation of the mesomorphic architecture of CNC in a polymerized bulk, this chapter will also highlight thermal and mechanical characterizations of the produced novel composites of CNC with PHEMA.

2.2. Experimental Section

2.2.1. Materials

Cotton cellulose powder (Whatman, CF11) was used as the original cellulose material. Sulfuric acid (Nacalai tesque, Inc.) and polyethylene glycol (PEG) (number average molecular weight = 20000 ± 5000, Wako Pure Chemical Ind., Ltd.) were used as received. A dialysis tubing (cutoff molecular weight = 14000) was used for dialysis of the CNC/water suspension. 2-Hydroxyethyl methacrylate (HEMA) (Wako Pure Chemical Ind., Ltd.) was purified by distillation. A photo-polymerization initiator, 2-hydroxy-2-methylpropiophenone (HMPPh) (Sigma-Aldrich), was used as received.

2.2.2. Preparation of CNC

Cellulose powder (7 g) was hydrolyzed with 65 wt % sulfuric acid (100 ml) in a separable flask equipped with a mechanical stirrer at 70 °C for 15 min. Subsequently, the system was diluted with an excessive amount of distilled water and cooled with iced water for about 15 min, to stop the hydrolysis reaction. The fluid dispersion thus obtained was centrifuged and the supernatant was removed. The refinement cycle of dilution and centrifugal separation was repeated until the suspension was uniformly turbid right after centrifugation. The resulting suspension was then dialyzed in distilled water until the pH value rose to ~5. Finally, the membrane tube dialyzing the suspension was immersed into a 7 wt % PEG aqueous solution for 3 days to obtain a concentrated CNC/water suspension. The concentration of CNC in the suspension was determined by measuring the weight of an aliquot of the suspension before and after oven-drying.

2.2.3. Synthesis of PHEMA-CNC Composites

A concentrated CNC/water suspension (usually CNC = 12–16 wt %) mentioned above, HEMA (monomer), and distilled water (diluent) were mixed together and homogenized for about 2 min with a homogenizer Physcotron NS-51 (Microtec Co., Ltd.). The content of CNC was fixed to 5.0 wt % in the CNC/water/HEMA system used for composite synthesis.

The weight ratio of water/HEMA was adjusted to enter in a range of 0.46–1.1 : 1 (corresponding to 0.5–1.2 : 1 in volume). Even when water-rich proportions up to 2.2 : 1 (w/w) were adopted, it was possible to obtain the objective composites; however, at ratios of ≥2.5 : 1, the polymerization method shown below did no making of a visually clear solid film. The major preparations in this chapter were made with a water/HEMA mixed solvent of 1.0 : 1 (for samples of dynamic mechanical analysis (DMA)) or 0.46 : 1 (for others), unless otherwise specified.

HMPPh was added to the CNC suspension in water/HEMA at a concentration of 0.5 wt % to the amount of water/HEMA, followed by vigorous stirring of the mixture under shielding of light. HMPPh was less soluble in water, but compatible with the mixed solvent. After quiescent standing for 3 days at room temperature (25 °C), the suspension separated into isotropic (upper) and anisotropic (lower) phases. Polymerization of HEMA was carried out in different phase situations of the CNC suspension, in order to obtain three polymer composites: two derived from the fully separated isotropic and anisotropic phases, and the other from the primary non-separating mixture (in a stage of <2 h lapse after preparing). They were named PHEMA-CNC_{iso}, PHEMA-CNC_{aniso}, and PHEMA-CNC_{mix}, respectively.

The polymerization process was conducted with irradiation of UV light centering ~350 nm. For this purpose, a 10 W UV lamp FL10BLB-A (Toshiba Lightning & Technology Corp.) was used. Each phase of the suspension was poured into a Teflon-coated dish (ϕ = 50 mm) with a pipette, then irradiated for 2 h at a distance of ~50 mm from the light source in an atmosphere of N_2 gas (30–35 °C). After that, the polymerized system was oven-cured at 80 °C for 2 h under an N_2 flow. The films obtained were immersed overnight in CCl_4 to extract a trace amount of monomer, then dried again at 80 °C *in vacuo*. A PHEMA homopolymer film was similarly prepared for comparison. Some of the films of PHEMA-CNC composites and plain PHEMA were pressed modestly (~5 MPa) at 120 °C with a hot-pressing apparatus (SA-302, Tester Sangyo Co., LTD.), for the purpose of flattening the surface of the films; this was required particularly for DMA and tensile measurements.

2.2.4. Measurements

Optical characterization of CNC suspensions and PHEMA-CNC composites was made under a polarized optical microscope (POM), Olympus BX60F5. The particle dimension of CNC was determined by transmission electron microscopy (TEM) using JEOL JEM-1220. The sample for this observation was prepared on a microscope grid from a 1.3 wt % suspension of CNC in water, through staining with uranyl acetate, followed by drying. Fracture surfaces of PHEMA-CNC composites were observed by using a field emission scanning electron microscope (FE-SEM), Hitachi S-4800; the composites were fractured at liquid nitrogen temperature and sputter-coated with Pt-Pd before the observation.

Differential scanning calorimetry (DSC) was carried out on 5 mg samples with a Seiko DSC6200/EXSTAR6000 apparatus. The temperature proof-readings were calibrated with an indium standard. Thermal properties of the composites were usually analyzed in two scans, i.e., the first and second heating. The first heating scan was run at a rate of 20 °C/min from ambient temperature (25 °C) to 220 °C under a nitrogen atmosphere. The second heating scan was done again at 20 °C/min, after quick cooling to −100 °C following the first heating. The glass transition temperature, T_g, was read off as a temperature at the midpoint of a base-line shift in heat flow characteristic of the transition.

DMA measurements were conducted by using a Seiko DMS6100/EXSTAR6000 apparatus in tension mode. Strips of rectangular shape (ca. 20 mm × 5 mm × 0.4 mm) cut from the pressed films (see above) were employed. Prior to the measurement, the film specimens were sandwiched between hard card-board strips and heated in a vacuum oven at 135 °C for 10 min for relaxation of possible stresses. The temperature dependence of the dynamic storage modulus E' and loss modulus E'' were measured. The measuring conditions were as follows: temperature range, −50–220 °C; scanning rate, 2 °C/min; oscillatory frequency, 10 Hz.

FT-IR spectra were recorded on a Shimadzu IR Prestige-21 apparatus over a wavenumber range of 400–4000 cm^{-1} with a resolution of 4 cm^{-1} via accumulation of 100 scans. Polymer samples were ground and mixed with KBr at a concentration of ≤2 wt % in a ball mill QM-1 (Chromato Science Inc.), and the respective mixtures were quickly pressed into a flat shape with a presser QP-1 (Chromato Science Inc.).

A tensile mechanical test was conducted by using a Shimadzu Autograph AGS-1kNG

apparatus at 23 °C and 50 % RH. Specimens were prepared by cutting stripes (ca. 20 mm × 5 mm × 0.6 mm) from the pressed films. Prior to the test, the specimens were conditioned at 23 ± 2 °C and 50 ± 10 % RH for more than 2 days. The strain rate and span length were 10 mm/min and 10 mm, respectively. At least three strips of the same film were employed, to confirm the reproducibility of data.

2.3. Results and Discussion

2.3.1. Visual and Microscopic Observations of CNC Suspensions and Composites

Figure 2-1 shows a TEM micrograph of the CNC particles used as mesogen filler; this sampling was done from a 1.3 wt % CNC/water suspension. The mean dimension was calculated by averaging the data of 50 particles, as 94 nm (s. d., 41 nm) in length and 9 nm (s. d., 2 nm) in diameter; therefore, the axial ratio was around 10. As exemplified by this micrograph, no particularly large aggregates were observed, indicating that a good state of dispersion of CNC in the aqueous suspension was carried over to the grid specimen for TEM to a considerable extent. With regard to the CNC/water/HEMA system, any of the mixtures prepared (water/HEMA = 0.46–2.2 : 1) could also form a stable suspension with no precipitation of CNC aggregates. An adequate compatibility of the monomer with water would be indispensable for the good dispersion of CNC attainable even in the HEMA-rich solvent condition.

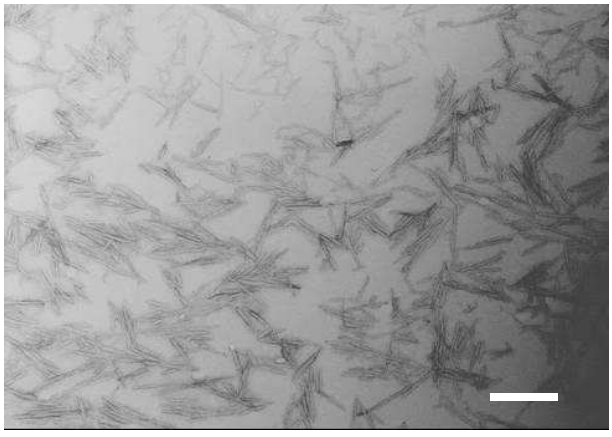

Figure 2-1. TEM image of CNC prepared by hydrolysis of cotton cellulose with concentrated sulfuric acid at 70 °C. Scale bar denotes 200 nm.

When CNC/water/HEMA suspensions were prepared at a concentration of 5.0 wt % CNC and allowed to stand quiescently at room temperature (25 °C), they habitually separated into an isotropic phase (upper part) and an anisotropic one (lower part) in 3 days after the preparation, as did the corresponding suspension in mere water. Concerning the critical CNC concentration (c_s) for the phase separation, however, it was somewhat elevated in the monomer solution (e.g., $c_s \approx 3.5$ wt % in water/HEMA of ~1.1 : 1), relative to the situation in mere water where c_s was a little less than 2.5 wt %. In POM observations, the anisotropic phase of the suspensions exhibited a fingerprint pattern spreading over the whole area of the optical image, as illustrated in Figure 2-2. This pattern is characteristic of cholesteric liquid crystals with a relatively long pitch in the helical arrangement of nematic directors. The repeating distance S_r of the so-called retardation lines making up the pattern is usually taken as corresponding to half the cholesteric pitch. For the example of a 5.0 wt % CNC/water/HEMA suspension given in Figure 2-2, S_r was estimated to be ca. 4.3 μm; however, the value tended to increase with increasing proportion of water in the mixed solvent (S_r = ~7.0 μm in water only). It was also confirmed qualitatively that S_r varied with CNC concentration in a manner of negative dependence, in accordance with the observation demonstrated formerly for the purely binary system of CNC/water.[13]

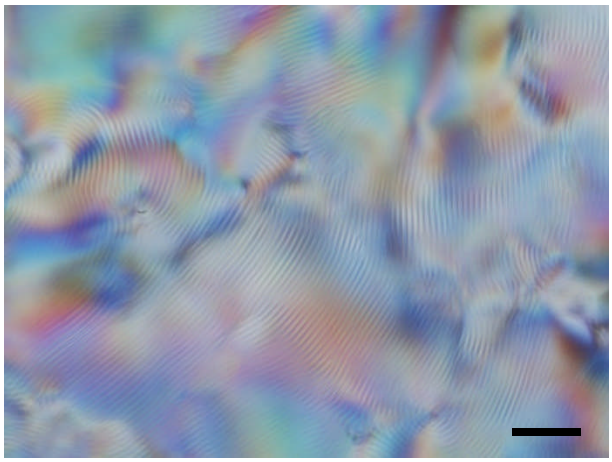

Figure 2-2. Polarized optical micrograph of the anisotropic phase of a 5.0 wt % CNC suspension in water/HEMA (0.46 : 1 in weight). Scale bar denotes 50 μm.

In consequence of the polymerization process described in the preceding section, the CNC/water/HEMA suspensions (5.0 wt % CNC; water/HEMA = 0.46–1.1 : 1) were successfully converted into PHEMA-CNC composites in a form of optically clear and rigid film. An example of the visual appearance is shown in Figure 2-3. The faintly yellowish color is derived from the photo-initiator HMPPh. In the preparation from a suspension in water/HEMA of 0.46 : 1, the CNC content in the three composite products may be assessed, as follows: PHEMA-CNC_{iso}, <7.1 wt %; PHEMA-CNC_{mix}, ~7.1 wt %; PHEMA-CNC_{aniso}, >7.1 wt %. In another solvent condition of 1.0 : 1, similarly, the CNC concentration for partitioning the three products is estimated at 9.5 wt %.

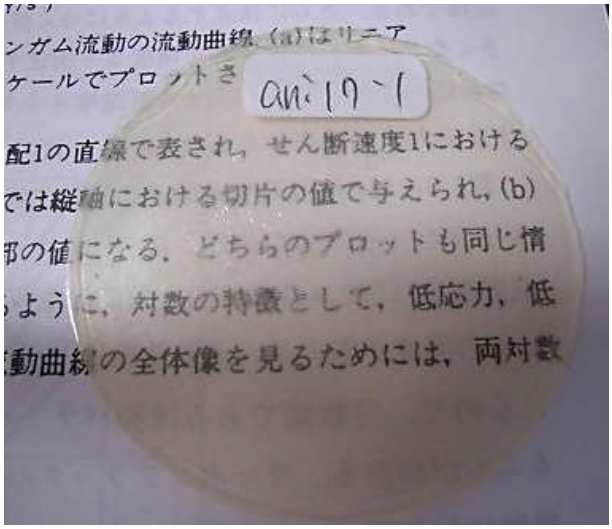

Figure 2-3. Visual appearance of a film of PHEMA-CNC_{aniso} obtained by polymerization of HEMA from the anisotropic phase (lower part) of a CNC/water/HEMA suspension (5.0 wt % CNC; water/HEMA = 0.46 : 1).

Figure 2-4 shows POM photographs of three composite films corresponding to the former set of PHEMA-CNC products just mentioned above; however, the samples were hot-pressed before the optical observation. All the composites are found to be, more or less, birefringent between crossed polars. As can be seen in Figures 2-4b and 2-4c, PHEMA-CNC_{iso} and PHEMA-CNC_{aniso} exhibited a fingerprint pattern, which was rather locally observed in the former and widely distributed in the latter. In the original phase-separated suspension, CNC particles in the isotropic phase would be comparatively shorter, while the longer ones would prefer being in the anisotropic phase.[14] This means that the distribution of CNC size becomes narrower in any of the two phases, relative to that in the non-separating mixture. As a result of the fractionation, even the CNC particles unaligned in the initially isotropic phase would easily associate with each other to form a cholesteric ordered domain in the process of polymerization of HEMA accompanied by condensation of the dispersoid due to evaporation of water. In the course of the evaporation, the sample should pass through a concentration range where the chiral nematic phase occurs; this kinetic effect must commensurately deposit the cholesteric organization of CNC in the film product. It is conceived thus that a fingerprint pattern appeared in PHEMA-CNC_{iso}.

For the two composites shown in Figures 2-4b and 2-4c, the line spacing of fingerprint was evaluated on the average as follows: S_r = 3.9 μm (for PHEMA-CNC_{iso}) and 3.5 μm (for PHEMA-CNC_{aniso}), both values diminishing from the corresponding data 4.3 μm observed for the anisotropic phase of the starting suspension.

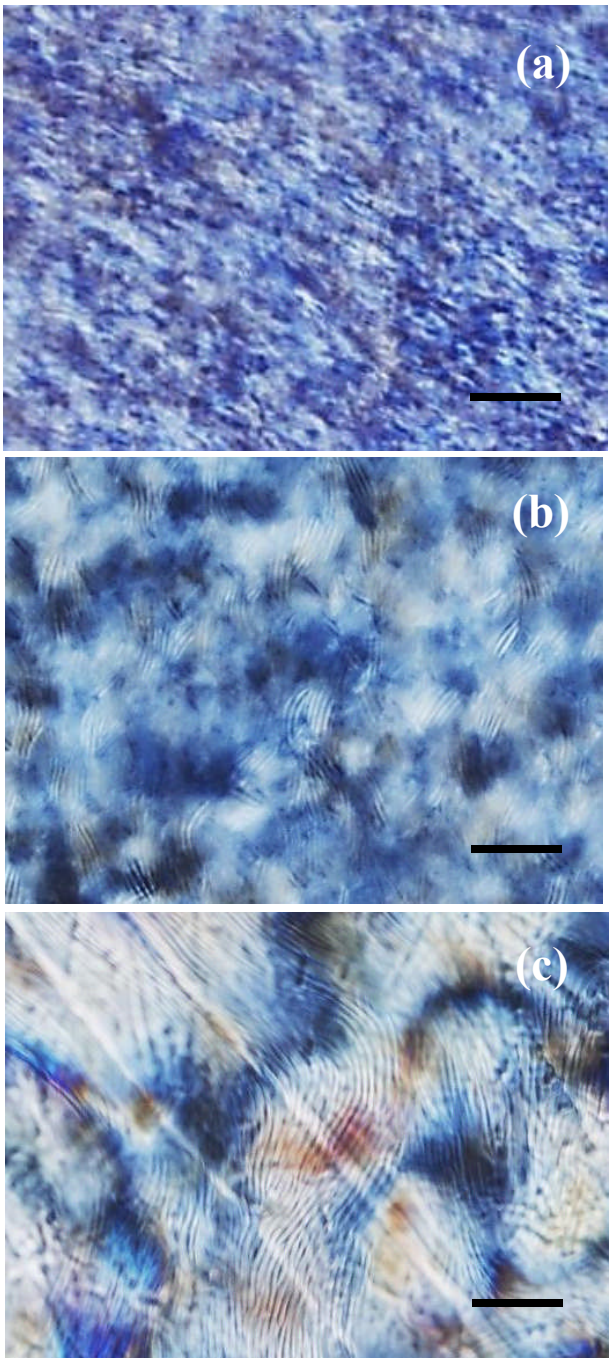

Figure 2-4. Polarized optical micrographs of hot-pressed films of polymer composites: (a) PHEMA-CNC_{mix}; (b) PHEMA-CNC_{iso}; (c) PHEMA-CNC_{aniso}. Scale bar denotes 50 μm.

These composites were also employed for examination of the internal morphology by FE-SEM. The result is given in Figure 2-5. Figures 2-5a and 2-5b illustrate fracture-surface images of PHEMA-CNC_{iso} and PHEMA-CNC_{aniso}, respectively, taken under lower magnification. Both data reveals the development of a periodically striated texture corresponding to the optical fingerprint pattern, but the texture observed for PHEMA-CNC_{iso} is much more defective in longitudinal persistency of the striations, in contrast with that for PHEMA-CNC_{aniso}. The periodic distance in the striated texture was estimated to be ~3.4 μm for PHEMA-CNC_{iso} and ~2.8 μm for PHEMA-CNC_{aniso}, each data being somewhat smaller than the corresponding S_r value obtained from the POM observation. This disagreement may be admitted, taking account of the difference in resolution power between the two microscopic techniques. Additionally, the samples for the FE-SEM observation were treated in liquid nitrogen, to offer the fracture surfaces.

FE-SEM investigation of the composite PHEMA-CNC_{aniso} was also conducted under higher magnification, as shown in Figures 2-5c and 2-5d. The micrograph in Figure 2-5d was taken for an area enlarging the period of 2.8 μm indicated by an arrow in Figure 2-5c. From the magnified view, we can see numerous fibrous entities embedded in a polymer matrix; their dimensions in diameter are comparable to those of CNC particles. Interestingly, they appear to align with changing the direction of their longer axis to make a helical rotation (see lines inserted as guides to the eye in Figure 2-5d). This alignment manner of the fibrils just corresponds to a cholesteric liquid-crystalline arrangement.

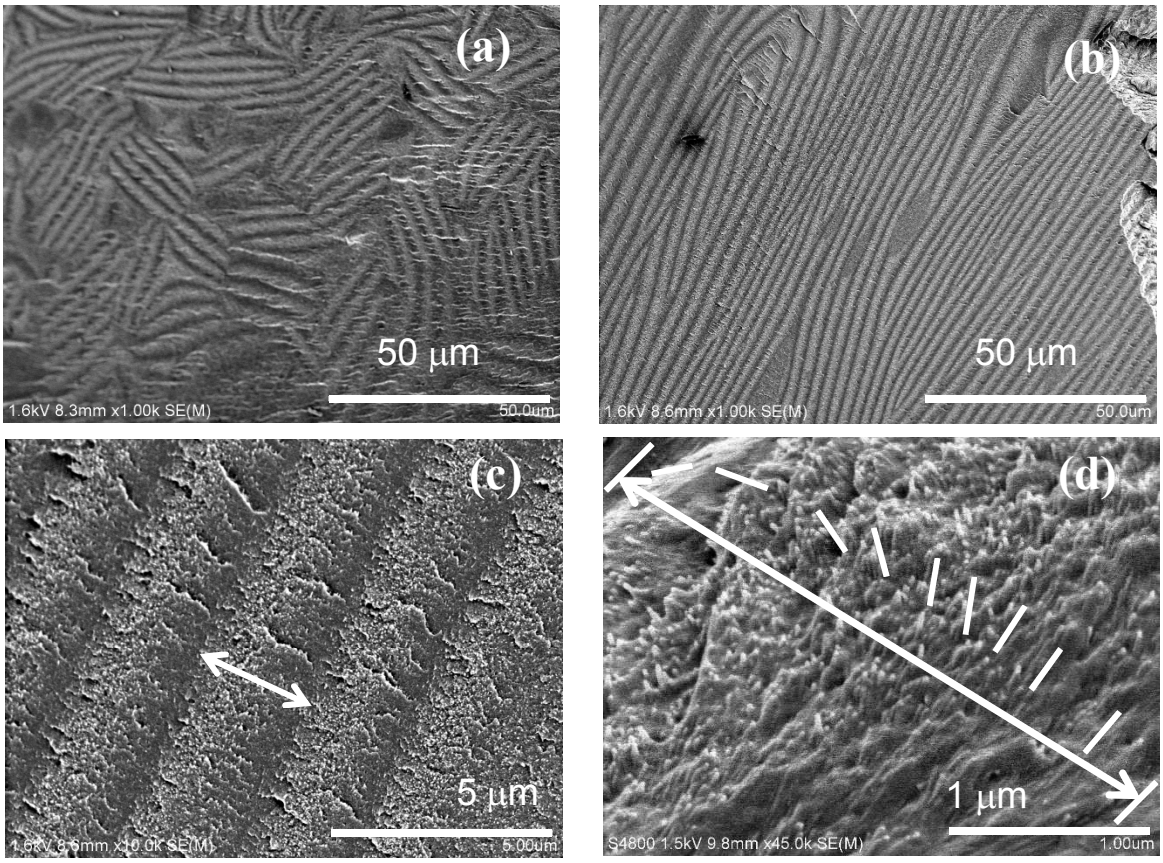

Figure 2-5. FE-SEM images of the fracture surfaces of polymer composites: (a) low-magnification data for PHEMA-CNC_{iso}; (b) low-magnification data for PHEMA-CNC_{aniso}; (c) enlarged view of (b); (d) enlarged view of an area accommodating the repeating distance indicated by an arrow in (c).

2.3.2. T_g Evaluation by DSC for Composites

Figure 2-6 compiles data of DSC thermal analyses conducted for the composite series of PHEMA-CNC and a reference sample of PHEMA homopolymer. Figure 2-6a compares four thermograms, all obtained in the second heating scan. In this scan, the plain PHEMA sample exhibited a clear base-line gap reflecting the glass transition and T_g = 104 °C was evaluated from the midpoint of the gap. Concerning T_gs of three composites PHEMA-CNC_{iso}, PHEMA-CNC_{aniso}, and PHEMA-CNC_{mix}, they were explicitly higher than that of PHEMA alone, but the former values (135–139 °C) were close to each other and the transition width in temperature was generally broaden in any of the three thermograms, as can be seen in Figure 2-6a.

Figure 2-6b compares two thermogramic curves observed in the first and second heating scans, respectively, for the reference PHEMA, and a similar comparison is made in Figure 2-6c for PHEMA-CNC_{mix}. In both figures, there appears an irregular curvature around 80 °C in the first DSC data, which is due to drying pretreatment at this temperature for many hours in the process of sample preparation (see Experimental Section). As is evident in Figure 2-6b, the plain PHEMA gave a midpoint T_g at 105 °C in the first scan, the value almost coinciding with that in the second. On the other hand, the composite PHEMA-CNC_{mix} provided a T_g value of 111 °C in the first heating scan; the T_g data is surely higher than that of PHEMA by several degrees, yet considerably lower than that (139 °C) in the second scan, as shown in Figure 2-6c. The same positional relation applied to T_g data for PHEMA-CNC_{iso} and PHEMA-CNC_{aniso}, and there was also no appreciable difference (<2 °C) in T_g between the three composites in the first heating series of DSC measurements.

In Figure 2-6c, we find a noteworthy thermal behavior; viz., the first DSC trace veers away to the endothermic direction at temperatures higher than 160 °C. This behavior was also observed in the first scans for PHEMA-CNC_{iso} and PHEMA-CNC_{aniso}, but never done for plain PHEMA (Figure 2-6b). In the corresponding temperature range, as proved below, those composites with CNC undergo a cross-linking reaction attended by dehydration, which would be mediated by the CNC dispersoids as acid catalyst. Probably, this reaction is responsible for the extraordinary divergence in heat flow mentioned above. Also, the quantification of a fairly high T_g in the second DSC scan for the composites may be attributed to the effect of cross-link formation in the first heating process.

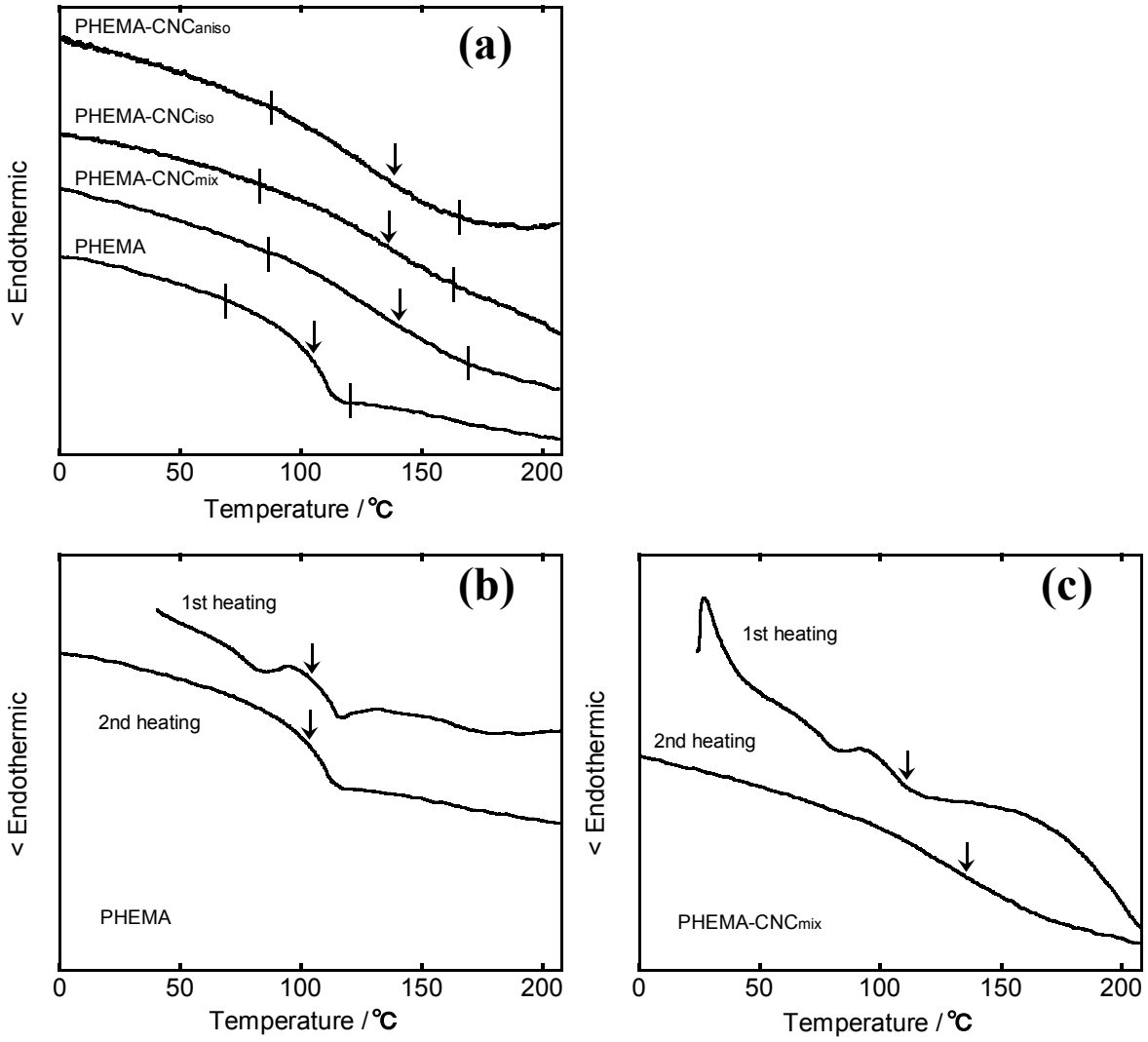

Figure 2-6. DSC thermograms of PHEMA and its composites with CNC: (a) data for PHEMA, PHEMA-CNC_{aniso}, PHEMA-CNC_{iso}, and PHEMA-CNC_{mix}, all obtained in the second heating scan; (b) data for PHEMA, compared between the first and second heating scans; (c) data for PHEMA-CNC_{mix}, compared between the first and second heating scans. Arrows indicate a midpoint T_g for each sample.

2.3.3. Dynamic Mechanical Analysis of Composites

DMA results for film samples of PHEMA and PHEMA-CNC composites are presented in Figure 2-7. Figure 2-7a collects four sets of data of the storage modulus E' and loss modulus E'' as a function of temperature, and the E'' data are re-plotted in Figure 2-7b by displacing by 0.25 log unit in the ordinate to be able to discern the respective peak maxima. The PHEMA film as reference exhibited a primary dispersion peak centering 115 °C in the E'' versus temperature curve; this dispersion can be associated with the glass transition of the homopolymer sample. A secondary dispersion due to a local relaxation mode was also discernible around 40 °C as a weak and broad shoulder in the E'' curve. The primary E''-peak is situated at a temperature higher than T_g (105 °C) determined by DSC, indicating that the two analytical tests responded somewhat differently to the same relaxation process.[15] Concerning the reference PHEMA, an important observation is the rapid and intense falls of E' and E'' in the glass transition region, reflecting the activity in micro-Brownian motion of the polymer chains, enhanced more and more with elevating temperature after onset of the transition on heating.

As made clearer in Figure 2-7b, the respective E'' curves for the composite samples used produce a peak maximum at a temperature of 123–127 °C, which is higher by ~10 °C than the corresponding temperature for the reference PHEMA. However, it is difficult to precisely specify the rank order of the upward shift between the three composites. The 10 °C ascent is of a little bit larger degree compared with the T_g elevation (~5 °C) noted in the DSC study (1st run); this difference in increment may be attributed to a somewhat higher CNC concentration in the respective composites used for this DMA measurement.

More significant changes in the thermo-mechanical property of PHEMA by the locking-in of CNC assemblies can be seen in the E' data for the composites. First, the moduli of the composites were always higher than that of the plain PHEMA in their respective glassy states, as shown on an enlarged scale in an inset of Figure 2-7a. As a general trend, the effectiveness of composition in raising the glassy modulus of the methacrylate polymer was pronounced in the order of PHEMA-CNC_{iso} ≤ PHEMA-CNC_{mix} < PHEMA-CNC_{aniso}; this order apparently corresponds to that of the CNC content allotted according to the three different phase conditions of the suspension to be polymerized. Secondly, most important, the CNC incorporation led to a drastic suppression of the E'-drop

in the glass transition region, in contrast to the rapid declining behavior of PHEMA alone, as evidenced in Figure 2-7a; the remark is also applicable to the E'' data. These DMA results clearly demonstrate that the dispersoid CNC component acts as an effective reinforcer for the polymer matrix, so as to improve the thermo-mechanical performance.

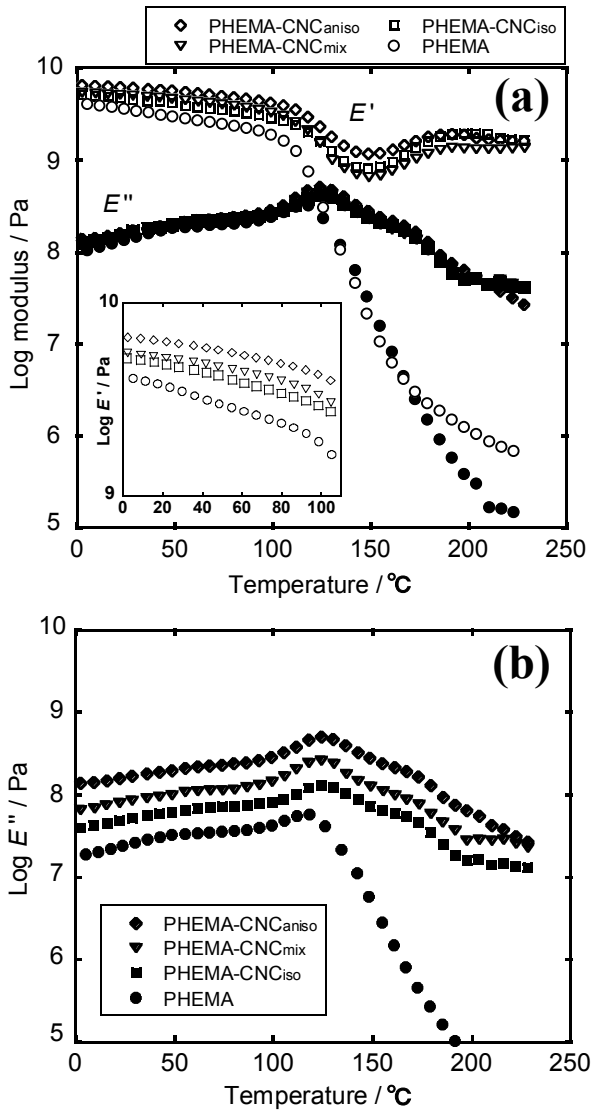

Figure 2-7. Temperature dependence of the storage modulus (E') and loss modulus (E''), measured for film samples of PHEMA and three PHEMA-CNC composites: (a) data in a set of E' and E'' for each sample, and an enlarged plot of the glass-state modulus E' (inset); (b) E'' data plotted by displacing by 0.25 log unit in the ordinate. See text for comparative discussion.

An additional interest in the present DMA data is the following observation: viz., the modulus *E′* of the respective composites re-increased with temperature in a range of ca. 150–190 °C, and then it became constant to make a plateau region. The unusual re-rise of the modulus may be interpreted as a transient process of some cross-linking reaction at the high temperatures of >150 °C. In order to confirm the cross-link formation, the author carried out a comparative FT-IR analysis by using small pieces from films of PHEMA-CNC_{aniso} and PHEMA *per se*. Four fragments from each film were once preheated at 135 °C for 10 min in a vacuum oven and then separately heated from 30 °C to a prescribed temperature of 100, 150, 200, and 250 °C at 2 °C/min in the DSC apparatus. After being taken out from the DSC pan, the fragments were powdered to prepare a KBr pellet for the FT-IR measurement. The spectra obtained are collected in Figure 2-8.

As shown in Figure 2-8a, the spectra of the four specimens of PHEMA were essentially identical, irrespective of the different thermal histories in sampling. In contrast to this, as demonstrated in Figure 2-8b, the heat treatment of the composite PHEMA-CNC_{aniso} gave rise to a definite change in absorbance of the IR signals in which hydroxyl groups participated, particularly conspicuous when the treating temperature was ≥150 °C. The composite specimen heated to 100 °C provided a spectral chart parallel to that of the PHEMA reference, although there was a small increase in intensity of the O-H stretching band centering 3450 cm^{-1} due to the addition of more than 7 wt % CNC particles. As the heat-treatment temperature was heightened from 150 to 250 °C, the O-H band became suppressed to a considerable extent. Also, two absorption peaks located at 1073 and 1015 cm^{-1} became seriously blunt; the IR signals are associated with a couple of stretching modes of the hydroxylethyl group of PHEMA. In concomitants with these declining effects, an absorption band centered at 1162 cm^{-1} became broadened with retaining an appreciable relative intensity; usually, IR responses to asymmetrical and symmetrical stretching vibrations of C-O-C linkages occupy the corresponding wavenumber range of 1250–1100 cm^{-1}.

From these observations, it can be reasonably deduced that, above ~150 °C, the composite undergoes a dehydration reaction accompanied by formation of ether cross-linkages:

$2PHEMA\text{-}(CH_2)_2\text{-}OH \rightarrow PHEMA\text{-}(CH_2)_2\text{-}O\text{-}(CH_2)_2\text{-}PHEMA + H_2O$

This reaction should be catalyzed by the acidic $CNC\text{-}OSO_3^- \cdot H^+$, judging from no indication of the structural change in the mere PHEMA specimens. If the dispersed CNC particles have some amounts of residual hydroxyls on their surfaces, a cross-linkage of

PHEMA-$(CH_2)_2$-O-CNC may also be possible.

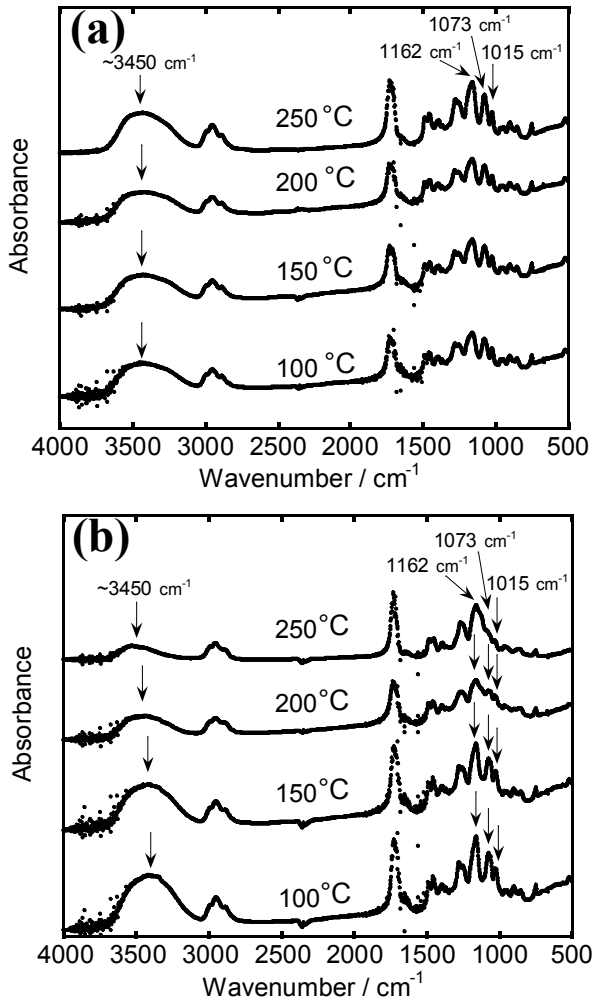

Figure 2-8. FT-IR spectra of PHEMA and PHEMA-CNC_{aniso}, measured after four fragments of each film were heated from 30 °C to a prescribed temperature of 100, 150, 200, and 250 °C, respectively, at 2 °C/min in a nitrogen atmosphere: (a) data for PHEMA; (b) data for PHEMA-CNC_{aniso}.

2.3.4. Tensile Behavior of Composites

In general, polymer materials are stiffened by compatible incorporation with rigid fillers.[16] This may also be applicable to the present composites of PHEMA-CNC, as was suggested in advance by the glass-state E' data higher than that of PHEMA homopolymer. To ensure such a stiffening effect by the CNC reinforcer, a tensile test was carried out on film specimens of PHEMA and three CNC-filled composites under an ambient condition of 23 °C and 50 % RH. Table 2-1 compiles average data of Young's modulus, elongation at rupture, and tensile strength. Figure 2-9 illustrates representative stress-strain curves obtained for PHEMA, PHEMA-CNC_{aniso}, and PHEMA-CNC_{mix}.

As can readily be recognized from the tensile data, any of the composite films showed a higher modulus relative to that of plain PHEMA, substantiating the attainment of a hard elasticity of the composites against extension. As is usual with many particulate-filled materials,[16] the present compositions commonly invited a lowering in the elongation at rupture; yet, it is worthy of remark that the strength of the composite PHEMA-CNC_{aniso} surpassed those of all the other samples tested. With regard to the two composites PHEMA-CNC_{iso} and PHEMA-CNC_{mix}, it was actually difficult to place either the second best in mechanical performance, although mostly the latter composite showed a little bit higher strength. In the preparations of these composite films, PHEMA-CNC_{mix} contained a higher concentration of CNC compared with PHEMA-CNC_{iso}, but the development of liquid-crystalline ordered structure was immature in PHEMA-CNC_{mix} rather than in PHEMA-CNC_{iso}, as has been revealed by microscopic observations.

Table 2-1. Tensile Mechanical Data for Films of PHEMA and PHEMA-CNC Composites

	Young's modulus / GPa	Elongation at rupture / %	Tensile strength / MPa
PHEMA	1.28	4.66	44.0
PHEMA-CNC_{iso}	1.84	2.41	36.3
PHEMA-CNC_{mix}	1.58	2.76	38.4
PHEMA-CNC_{aniso}	2.03	2.92	46.3

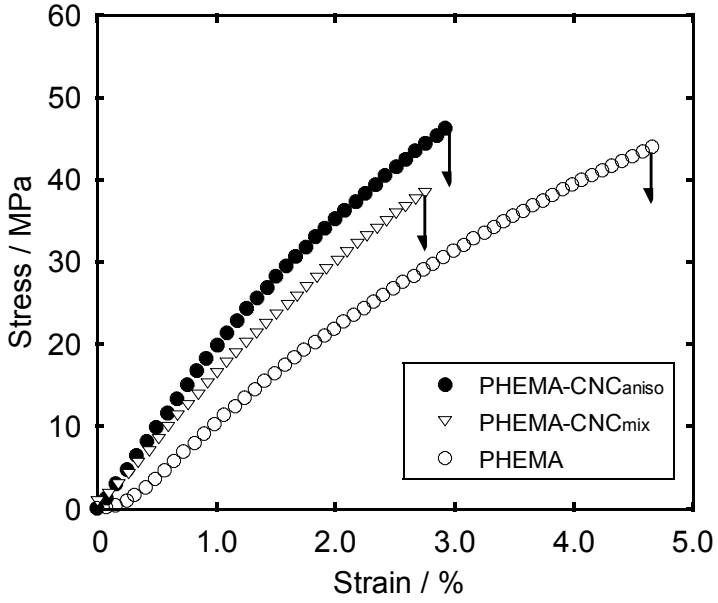

Figure 2-9. Examples of stress-strain curves measured for films of PHEMA, PHEMA-CNC_{aniso}, and PHEMA-CNC_{mix}.

References

(1) Revol, J. -F.; Bradford, H.; Giasson, J.; Marchessault, R. H.; Gray, D. G. *Int. J. Biol. Macromol.* **1992**, *14*, 170–172.

(2) Guo, J. -X.; Gray, D. G. Chapter 2. In *Cellulosic Polymers, Blends and Composites;* Gilbert, R. D., Ed.; Hanser: Munich/New York, 1994.

(3) Orts, W. J.; Godbout, L.; Marchessault, R. H.; Revol, J. –F. *Macromolecules* **1998**, *31*, 5717–5725.

(4) Favier, V.; Chanzy, H.; Cavaillé, J. Y. *Macromolecules* **1995**, *28*, 6365–6367.

(5) Azizi Samir, M. A. S.; Alloin, F.; Sanchez, J. -Y.; El Kissi, N.; Dufresne, A. *Macromolecules* **2004**, *37*, 1386–1393.

(6) Petersson, L.; Kvien, I.; Oksman, K. *Compo. Sci. Tech.* **2007**, *67*, 2535–2544.

(7) Li, Q.; Zhou, J.; Zhang, L. *J. Polym. Sci., Part B: Polym. Phys.* **2009**, *47*, 1069–1077.

(8) Revol, J. -F.; Godbout, L.; Gray, D. G. *J. Pulp Pap. Sci.* **1998**, *24*, 146–149.

(9) Viet, D.; Beck-Candanedo, S.; Gray, D. G. *Cellulose* **2007**, *14*, 109–113.

(10) Nishio, Y.; Hirose, N. *Polymer* **1992**, *33*, 1519–1524.

(11) Miyashita, Y.; Nishio, Y.; Kimura, N.; Suzuki, H.; Iwata, M. *Polymer* **1996**, 37, 1949–1957.

(12) Miyashita, Y.; Kimura, N.; Suzuki, H.; Nishio, Y. *Cellulose* **1998**, *5*, 123–134.

(13) Beck-Candanedo, S.; Roman, M.; Gray, D. G. *Biomacromolecules* **2005**, *6*, 1048–1054.

(14) Dong, X. M.; Revol, J. -F.; Gray, D. G. *Cellulose* **1998**, *5*, 19–32.

(15) Macknight, W. J.; Karasz, F. E.; Fried, J. R. Chapter 5. In *Polymer Blends, Vol. 1;* Paul, D. R., Newman, S., Eds.; Academic Press: New York, 1978.

(16) Nielsen, L. E. Chapter 7. In *Mechanical Properties of Polymers and Composites;* Marcel Dekker: New York, 1975.

Chapter 3
Anisotropic Polymer Composites Synthesized by Immobilizing Cellulose Nanocrystal Suspensions Specifically Oriented under Magnetic Fields

3.1. Introduction

Cellulose nanocrystals (CNCs) attract increasing attention in the broad field of material science and technology. The bio-derived nanoparticles are favorable in the contexts not only of abundance, biodegradability, and renewability but also of well-defined dimension and excellent mechanical properties.[1,2] Actually, CNCs are characterized by the high tensile strength (~7.5 GPa) and elastic modulus (~150 ± 50 GPa),[3,4] and the high aspect ratio involving diameters of ~5 to several tens of nanometers and lengths of ~100 nm to a few micrometers, both dimensions variable depending on the cellulose source.[1] The combination of the high modulus and strength with the high aspect ratio should make CNCs ideal fillers to reinforce a variety of polymer solid materials, leading to development of high-performance nanocomposites. Since the early demonstration by Favier et al. in 1995,[5,6] really many studies have been devoted to fabricating nanocomposites by incorporating CNC into various polymers including starch, poly(lactic acid), silk fibroin, cellulose acetate butyrate, poly(styrene-*co*-butyl acrylate), poly(vinyl chloride), polypropylene, poly(oxyethylene), poly(vinyl alcohol), etc.[1–4]

Another specific property of CNCs is to form a self-ordering structure in their aqueous suspensions.[7–10] The nanoparticles are conventionally prepared by acid hydrolysis of native cellulose fibers with sulfuric acid, and then the surfaces of the resultant CNCs are each sulfated. The rod-like shape and negative surface charge of CNCs give rise to an electrostatically stable colloidal suspension in water; the suspension system phase-separates into an upper random phase (isotropic) and a lower ordered phase (anisotropic) at CNC concentrations above a critical value, typically 3–5 wt % for cotton-derived CNCs. The anisotropic phase is optically birefringent and exhibits a chiral nematic (or cholesteric) arrangement of CNC constituents, as do the molecular mesophases of many liquid-crystalline cellulose derivatives.[11]

Despite fascination of the ordering property of CNCs, the major examples of their use as

reinforcing agent have been limited to the random- or poorly oriented state of CNC dispersion in polymer matrices. Recently, however, some researchers of polymer composites have begun to focus interest on desirable performances and/or specific functions arising from anisotropic alignments of the stiff CNC fillers. One approach to CNC orientations is draw deformation. For instance, CNC rods were successfully aligned in deformed aqueous media containing water-soluble polymers,[12,13] to yield dried polymer-CNC nanocomposites showing an enhanced mechanical performance in the draw direction. Another effective way to achieve CNC alignment is the application of a strong magnetic field[14–16] and this non-contact technique is useful regardless of the outer shape of materials. In fact, a unidirectionally reinforced nanocomposite was demonstrated for poly(vinyl alcohol)-CNC[17] and cellulose-CNC (all-cellulose composite)[18] systems which were prepared in film form by solution casting under the action of a static magnetic field.

Generally, fibers with diamagnetic anisotropy align under static magnetic fields so that the axis of the largest diamagnetic susceptibility χ_1 (<0) lies parallel to the applied field. In cellulose fibers and nanocrystals, this axis (often termed the axis of easy magnetization) is perpendicular to the longitudinal axis of the fibrous entities.[15,19] Uniaxial alignment of the smallest diamagnetic susceptibility (χ_3 ($<\chi_1$)) axis (the axis of hard magnetization) can be accomplished by using a rotating magnetic field,[20] which is applicable not only to the fiber suspensions but also to many other rheological systems possessing negative anisotropic diamagnetic susceptibilities. Kimura et al. previously reported on such a uniaxial magnetic alignment of CNCs attainable for the mesomorphic ordered suspensions.[21] Furthermore, three-dimensional alignment of crystalline powders was enabled by the use of dynamically modulated (elliptical) magnetic fields,[22] and thus an attempt was also made to prepare a pseudo single crystal of cellulose.[23]

In a preceding chapter,[24] the authors demonstrated the successful synthesis of novel composites comprising CNCs and poly(2-hydroxyethyl methacrylate) (PHEMA) from CNC suspensions in an aqueous 2-hydroxyethyl mechacrylate (HEMA) monomer solution. The starting suspensions (~5 wt % CNC) separated into an isotropic upper phase and an anisotropic bottom one in the course of standing. By way of polymerization of HEMA in different phase situations of the suspensions, the authors obtained films of three polymer composites, PHEMA-CNC_{iso}, PHEMA-CNC_{aniso}, and PHEMA-CNC_{mix}, coming from the isotropic phase, anisotropic phase, and initial nonseparated suspension, respectively. Any of

the CNC incorporations into the PHEMA matrix improved the original thermal and mechanical properties of this amorphous polymer material. The mechanical reinforcement effect of the CNC dispersions was ensured in a tensile test, whereby PHEMA-CNC_{aniso} was found to surpass the other two composites in stiffness and strength.

In this chapter, the authors adopted the magnetic alignment technique in order to accentuate the impact of CNC alignment on physical properties of PHEMA-CNC composites. Effort was made to synthesize variously oriented CNC composites from the anisotropic and isotropic suspensions of CNC/water/HEMA to which a controlled static or rotational magnetic field was applied. The orientation states of CNC in the prepared composites were characterized by polarized optical microscopy, scanning electron microscopy, and wide-angle X-ray diffraction (WAXD). Dynamic mechanical analysis (DMA) was performed by artifice to assess the mechanical anisotropy of the composites.

3.2. Experimental Section

3.2.1. Preparation of CNC Suspensions

CNCs of an average size 95 nm long and 9 nm wide were isolated from cotton cellulose powder (Whatman, CF11) by acid hydrolysis. The detailed procedure was described in the preceding chapter.[24] Briefly, cellulose powder was hydrolyzed with 65 wt % sulfuric acid (Nacalai tesque, Inc.) at 70 °C for 15 min. The fluid dispersion once obtained was refined with the cycle of dilution and centrifugal separation. The resulting suspension was put into a membrane tube and dialyzed in distilled water, then concentrated by immersing the tube into an aqueous solution of 7 wt % polyethylene glycol (number average molecular weight = 20000 ± 5000, Wako Pure Chemical Ind., Ltd.). Sulfur content of the prepared CNCs was determined to be ~1.0 wt % by titration of the acid particles against 0.01 M sodium hydroxide solution, by reference to a way described by Dong et al.[10]

The procedure for preparing CNC suspensions in aqueous methacrylate monomer was also explained before.[24] In brief, a concentrated CNC/water suspension (usually CNC = 16–23 wt %) mentioned above was mixed with 2-hydroxyethyl methacrylate (HEMA; Wako Pure Chemical Ind., Ltd., purified by distillation) and distilled water (diluent), and homogenized for 2 min. The content of CNC was fixed to ~6.0 wt % in the CNC/water/HEMA system. The weight ratio of water/HEMA was adjusted to about 0.56 : 1 (corresponding to 0.60 : 1 in volume). Subsequently, a photo-polymerization initiator, 2-hydroxy-2-methylpropiophenone (HMPPh; Sigma-Aldrich) was added to the mixture at a concentration of 0.5 wt % to the amount of water/HEMA, followed by vigorous stirring under shielding of light. After quiescent standing for 3 days at room temperature (25 °C), the CNC suspension separated into isotropic (upper) and anisotropic (lower) phases in a glass container. The volume fraction of the lower anisotropic phase was ~0.6, approximated with a tolerance of 5 %.

3.2.2. Magnetic Orientation and Composite Synthesis

An anisotropic or isotropic suspension sample, pipetted off from the parent CNC suspension (see above), was poured into a Teflon-coated dish (50 mm diameter and 10 mm height) exclusively for application of a static magnetic field (Figure 3-1a) or into a polyethylene (PE) cylindrical container (9 mm diameter and 10 mm height) for any use of static and rotational magnetic fields (Figure 3-1b). After that, the dish or PE cylinder was placed at the center of a cryocooler-cooled superconducting magnet (Sumitomo Heavy Industries, Ltd.) generating an 8 T horizontal magnetic field. To make a rotational field, the PE container was mounted on a homebuilt sample rotator with a vertical shaft rotatable at the center of the horizontal static field arising inside the magnet apparatus. The rotation velocity (ω) of the sample rotator was variable, but, by preference, a constantly rotating magnetic field of ω = 150 rpm and the static 8 T magnetic field (ω = 0) were each applied to the suspensions at ~25 °C for 2 h in the present comparative study. An attempt was also made to use an elliptical magnetic field, i.e., a periodically modulated rotation of magnetic field. For this purpose, two rotation velocities ω_1 and ω_2 were used in the angular ranges α and 180°−α, respectively, as represented in Figure 3-1b; in practice, ω_1/ω_2 = 40/160 or 20/140 (in rpm/rpm) was adopted in the angular variations of α = 20, 60, and 90°.

Various distribution states of CNCs magnetically oriented in the suspensions were immobilized by UV-induced polymerization of HEMA in two steps. Right after the application of a prescribed magnetic field for 2 h, first, the oriented CNC suspension was irradiated with UV light of 365 nm for 15 min at a distance of ~30 mm from the light source (Hamamatsu Photonics K.K., L5662) which was set up inside of the magnet apparatus purged with N_2 gas. Subsequently, the pretreated sample was taken out from the magnet, then again irradiated with UV light centering ~350 nm for 2 h by using a larger UV lamp, 10 W FL10BLB-A (Toshiba Lightning & Technology Corp.). In the second irradiation, the sample was placed at a distance of ~50 mm from the light source in an atmosphere of N_2 gas. After that, the polymerized system was oven-cured at 80 °C for 1 h under an N_2 flow. The PHEMA-CNC composites thus obtained were immersed overnight in CCl_4 to extract a trace amount of monomer, then dried again at 80 °C in vacuo. To encode the applied magnetic field in their sample names, the notation -s (static), -r (rotational), or -e (elliptical) is added to the previously used names PHEMA-CNC_{aniso} and PHEMA-CNC_{iso}. For example,

PHEMA-CNC_{aniso}-r denotes a composite synthesized by application of the rotational magnetic field (ω = 150 rpm) to the anisotropic mesophase of CNC and subsequent polymerization of the solvent HEMA. For samples of PHEMA-CNC_{aniso}-e, the authors termed them with additional codes indicating the combined frequencies ω_1/ω_2 and the angular range α, for example, as PHEMA-CNC_{aniso}-e-40/160-90 when ω_1/ω_2 = 40/160 rpm/rpm and $\alpha = 90°$.

PHEMA-CNC composites prepared in film form with the larger dish were cut into rectangular strips, and cylindrical composites prepared with the PE container were cut into a cubic shape; these processes were appropriate for examinations by DMA, etc. (see below). For the sake of convenience, a coordinate system O-$X_I X_{II} X_{III}$ was fixed to each oriented sample, as shown in Figure 3-1c; let the X_{III}-axis be parallel to the vector $\boldsymbol{B}$ of the static magnetic field and the X_I-axis be a normal ($\boldsymbol{N}$) to the plane (O-$X_{II}X_{III}$) of the rotational magnetic field. For reference, film samples and cylindrical (then cuboid) ones of PHEMA and PHEMA-CNC_{aniso} were also prepared under no magnetic field.

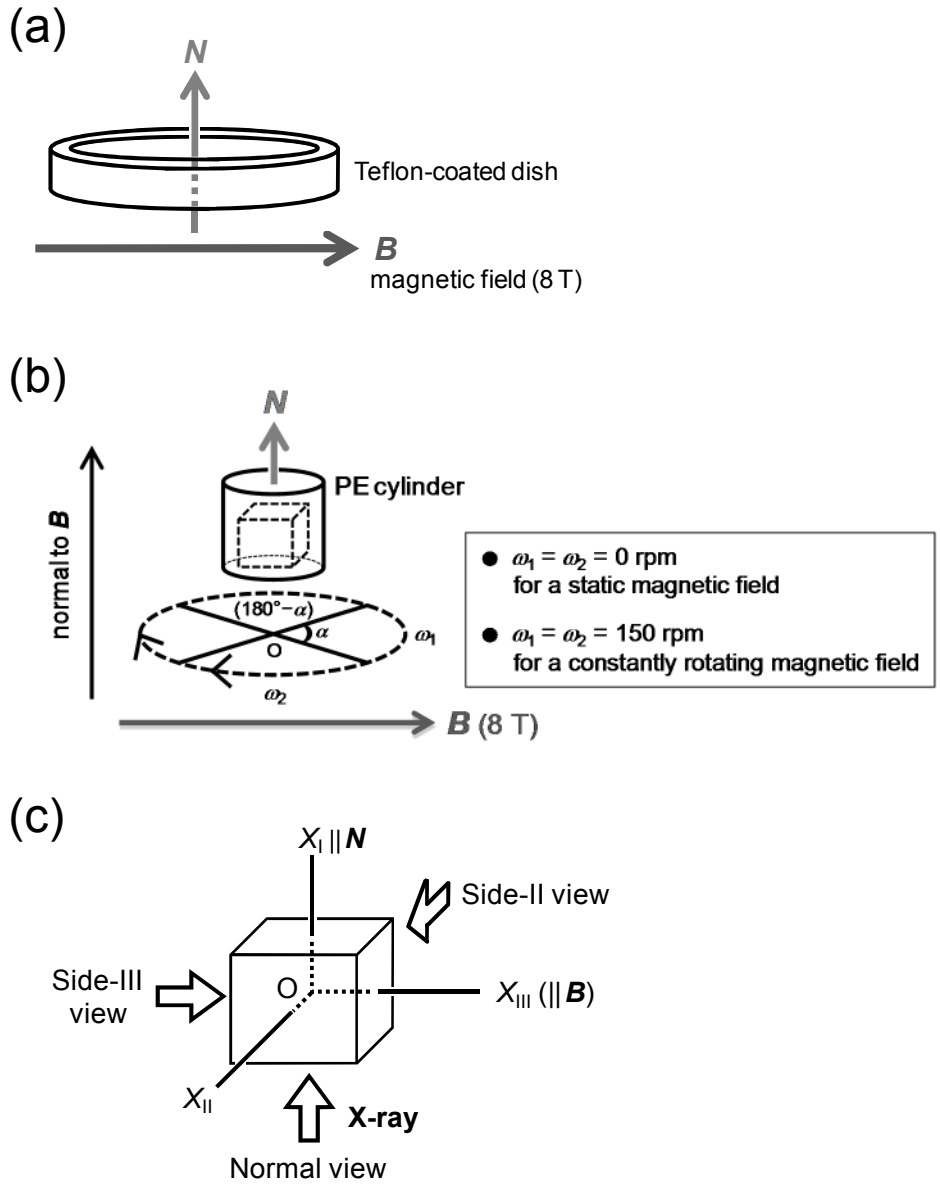

Figure 3-1. Schematic illustrations of the magnetic alignment systems using an 8 T field ***B***: (a) application of a static magnetic field for preparing samples in film form; (b) applications of diverse magnetic fields for preparing samples in cylindrical form ($\omega_1 = \omega_2 = 0$ for a static magnetic field and $\omega_1 = \omega_2 = 150$ rpm for a constantly rotating magnetic field); (c) setting up of a coordinate system O-$X_I X_{II} X_{III}$ to each sample magnetically oriented, and definition of three views for WAXD measurements.

3.2.3. Measurements

Optical characterization of PHEMA-CNC composites was made under a polarized optical microscope (POM), Olympus BX60F5. For the sample slides, thin slices 2–3 μm thick were cut off from the original products by using a microtome, DuPont Instruments JB-4; the glass knife was moved parallel to the normal axis X_{I} ($\|\boldsymbol{N}$). Fracture-surface morphology of the composites was observed by using a field emission scanning electron microscope (FE-SEM), Hitachi S-4800; they were fractured at liquid nitrogen temperature and sputter-coated with Pt before the observation.

WAXD measurements were made using a MAC Science Dip 2000 diffractometer equipped with an MXP18HF22 rotating anode generator. The measuring conditions were as follows: voltage and current of operation, 45 kV and 84 mA; X-ray wavelength, 0.154 nm (Ni-filtered CuKα); collimator size, 0.90 mm; camera distance, 150 mm; exposure time, 1800 s. The diffraction patterns were obtained usually in three views different from each other in the direction of X-ray incidence, which was parallel to the axis X_{I} (normal view), X_{II} (side-II view), or X_{III} (side-III view), as indicated by white arrows in Figure 3-1c.

DMA measurements were conducted by using a Seiko DMS6100/EXSTAR6000 apparatus in tension or compression mode. Major samples in the tension-mode measurement were two strips of rectangular shape (ca. 20 mm × 5 mm × 0.4 mm) cut in mutually right-angled directions from the film products of PHEMA-$\mathrm{CNC}_{\mathrm{aniso}}$-s (see Figure 3-9a). Prior to the measurement, the film specimens were sandwiched between hard cardboards and heated in a vacuum oven at ~130 °C for 7 min for relaxation of possible stresses. On the other hand, cuboids with edges of 5–6 mm shaped from the cylindrical products of variously magneto-treated composites were employed for the measurements in compression mode (see Figure 3-9b). The cuboid specimens were also heat-treated in a vacuum oven at ~130 °C for 7 min before the measurement. In any of the modes, the dynamic storage modulus E' and loss modulus E'' were followed at an oscillatory frequency of 10 Hz usually in the temperature range of −40–220 °C, the temperature being raised at a rate of 2 °C/min. Reference samples of PHEMA and PHEMA-$\mathrm{CNC}_{\mathrm{aniso}}$ were also examined in a similar manner. All the measurements were duplicated, and there was no substantial difference between the DMA data for two specimens prepared in the same manner.

3.3 Results and Discussion

3.3.1. Microscopic Observations of PHEMA-CNC Composites

By polymerizing HEMA monomer in the CNC/water/HEMA suspensions after application of the desired magnetic field, PHEMA-CNC composites were successfully obtained in film or cylindrical form. Film samples (<0.5 mm thick) were transparent, whereas the cylindrical ones (9 mm diameter) were generally translucent due to the thickness. In the preparation from a 6.4 wt % CNC suspension in water/HEMA (0.56:1), for example, the CNC contents in the composite products derived from the two separated phases were evaluated as follows: PHEMA-CNC_{iso}, ~6.3 wt %; PHEMA-CNC_{aniso}, ~12.7 wt %. These were calculated from the CNC concentrations 4.1 and 8.6 wt % present in the isotropic and anisotropic phases, respectively, before polymerization.

Figure 3-2 shows POM images of two composites categorized as PHEMA-CNC_{aniso}-s (photo a) and PHEMA-CNC_{aniso}-r (photo b), both synthesized in the cylindrical shape. The PHEMA-CNC_{aniso}-s composite was birefringent and imparted a definite chiral nematic supramolecular organization, as evidenced in Figure 3-2a; viz., the slice sample exhibited an ordered fingerprint pattern with the so-called retardation lines running perpendicular to the applied magnetic field $\boldsymbol{B}$ and therefore with the chiral nematic helical axis oriented parallel to the field $\boldsymbol{B}$. The repeating line distance S_r corresponding to half the chiral nematic pitch was usually in a range of 3–5 μm, which made an imperceptible difference from an estimate of S_r = 3.5–4.0 μm for PHEMA-CNC_{aniso} references free of magneto-treatment. Essentially the same structural feature of regular fingerprints was observed for another PHEMA-CNC_{aniso}-s composite prepared in film form. In contrast, as illustrated in Figure 3-2b, slices of the PHEMA-CNC_{aniso}-r composite indicated no specific pattern derived from the chiral nematic mesophase; however, the composite was found to be a uniaxially anisotropic material with the optical axis lying in the direction $\boldsymbol{N}$ perpendicular to the plane of rotating magnetic field. This was confirmed from the observation of light transmission for the slice sample as a function of its rotation under the crossed polars ($\boldsymbol{P}\perp\boldsymbol{A}$) in POM; viz., setting the sample at the diagonal position ($\boldsymbol{N}$ making 45° with $\boldsymbol{P}$) gave rise to a maximum in brightness of the field of view, while the orthogonal positions of $\boldsymbol{N}||\boldsymbol{P}$ and $\boldsymbol{N}||\boldsymbol{A}$ resulted in extinction of the transmittance.

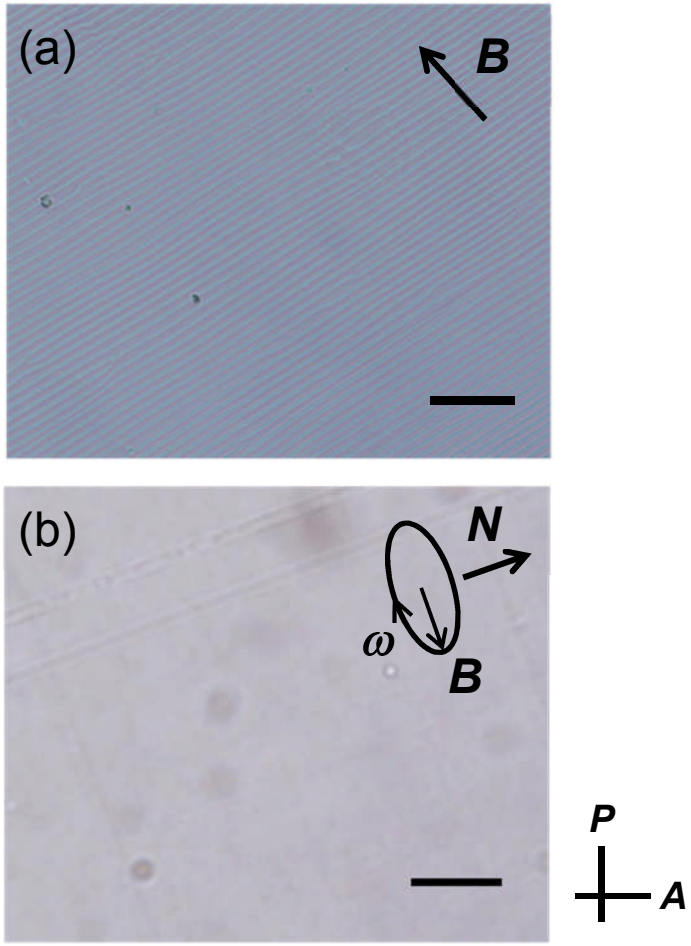

Figure 3-2. Polarized optical micrographs of thin slices of polymer composites: (a) PHEMA-CNC_{aniso}-s; (b) PHEMA-CNC_{aniso}-r, both synthesized in cylindrical form. Scale bar denotes 50 μm.

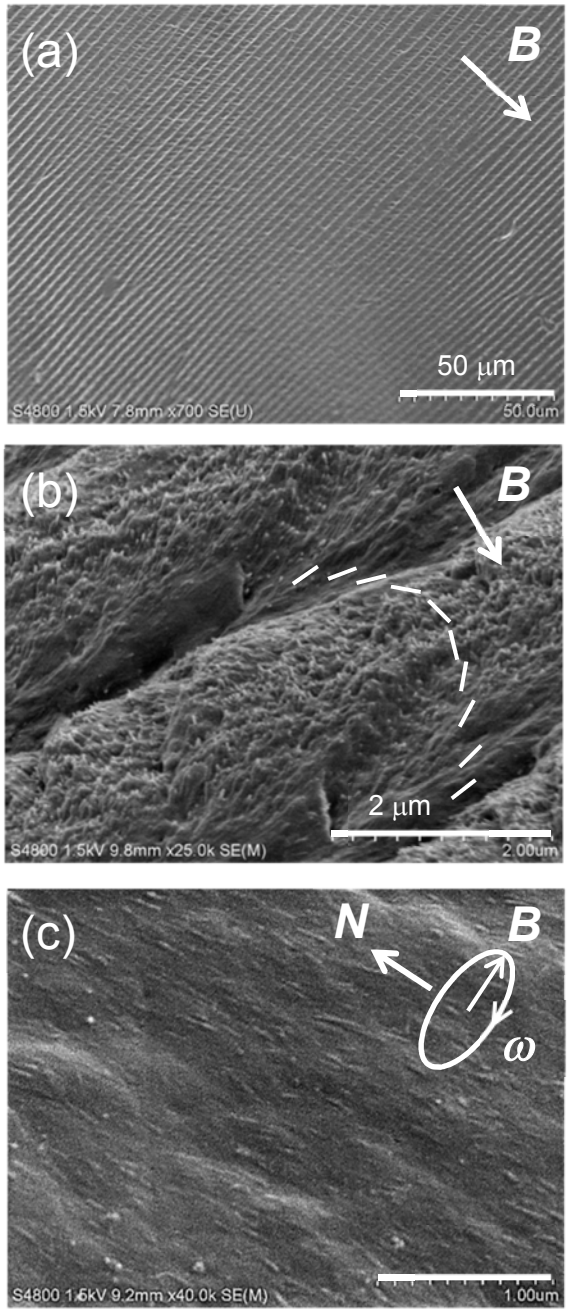

Figure 3-3. FE-SEM images of the fracture surfaces of polymer composites: (a) low-magnification data for PHEMA-CNC_{aniso}-s; (b) enlarged view of (a); (c) high-magnification data for PHEMA-CNC_{aniso}-r.

The composites of PHEMA-CNC_{aniso}-s and PHEMA-CNC_{aniso}-r were also fractured and the resulting surfaces were used for exploration of the internal morphology by FE-SEM. The typified results are given in Figure 3-3. Figure 3-3a reveals the development of a periodically striated texture corresponding to the optical fingerprint pattern in the PHEMA-CNC_{aniso}-s composite; the striations are found to be each well extended with a long persistency. In this image area, the periodic distance in the texture was estimated ~3.2 μm on average and the value was comparable to a data of S_r = ~3.5 μm obtained by POM observations for vicinal areas of the same composite. Figure 3-3b shows a higher magnification photomicrograph of the 3–3.5 μm periodicity appearing in Figure 3-3a. From the magnification, we can see numerous fibrous entities (CNC rods) embedded in a polymer matrix. The fibrils appear to make a helical rotation, as guided to the eye by lines inserted in Figure 3-3b; a left-handed chiral nematic arrangement of CNCs may be suggested from the arcing track.[25] Contrastively, the composite product of PHEMA-CNC_{aniso}-r exhibited no trace of such a chiral nematic structure; instead, as shown in Figure 3-3c, fibrous substances comparable to CNCs were observed to align in the direction normal to the rotation plane of $\boldsymbol{B}$.

When chiral nematic CNC suspensions are placed in a high magnetic field, generally, the longitudinal axis of CNC lies perpendicular to the field vector $\boldsymbol{B}$ because of the negative diamagnetic susceptibility and the supramolecular helix axis is aligned parallel to $\boldsymbol{B}$.[19] As two ideal schemes are drawn in Figure 3-4, the application of a static magnetic field can produce a uniform structure of chiral nematic monodomain,[19,21] whereas the use of a rotational magnetic field can realize an oriented nematic state, i.e., uniaxial alignment of CNCs, attended by unwinding of the initial helicoidal arrangement.[21] In the present study, it may be reasonably assumed from the POM and FE-SEM observations that the two types of CNC orientations were successfully achieved in the CNC/HEMA aqueous suspensions by the set-up of static and rotational magnetic fields and well fixed into the PHEMA-CNC_{aniso}-s and PHEMA-CNC_{aniso}-r composites via photo-polymerization of the corresponding magneto-treated suspensions.

The same static or rotational magnetic field was applied to isotropic CNC suspensions and PHEMA-CNC_{iso}-s and PHEMA-CNC_{iso}-r samples were prepared and characterized in similar manners. As a consequence, the microscopic observations revealed that both of the composites were quite poor in birefringence and CNCs were oriented nearly at random in the respective polymer matrices. Even for the isotropic suspension system, in principle, a planar

orientation of CNCs (perpendicular to ***B***) and a uniaxial orientation of CNCs (parallel to ***N***) should be possible by application of a static magnetic field and a rotational one, respectively. Nevertheless, such magnetic orientation effects were not realized for the isotropic suspensions under the present experimental conditions. Conversely, this result accentuates a more sensitive response of the mesomorphic assembly of CNCs to the magnetic stimuli; CNCs are originally oriented with some lateral coordination in the mesophase.

As regards the additional series PHEMA-CNC_{aniso}-e obtained under a magnetic field of modulated rotation of ***B***, the authors expected the investment of an optically biaxial anisotropy given rise to by a preferred orientation of CNC around its longitudinal axis.[23] However, the authors hardly discerned such a specific optical anisotropy for any of the PHEMA-CNC_{aniso}-e composites prepared in this study. Rather, for example, two samples of PHEMA-CNC_{aniso}-e-40/160-α (α = 60 and 90°) imparted a uniaxial orientation pattern of CNCs similar to that in the PHEMA-CNC_{aniso}-r composite (ω = 150 rpm), with accompanying conversion from the chiral nematic to nematic arrangement; this was confirmed by POM and FE-SEM techniques. Exceptionally, some traces of the fingerprints were partly observed in slice specimens of PHEMA-CNC_{aniso}-e-20/140-90. In this composite, probably, the rather lower average velocity of ***B*** rotation (ω_{ave}= 80 rpm) resulted in such an incomplete nematic alignment of CNCs.

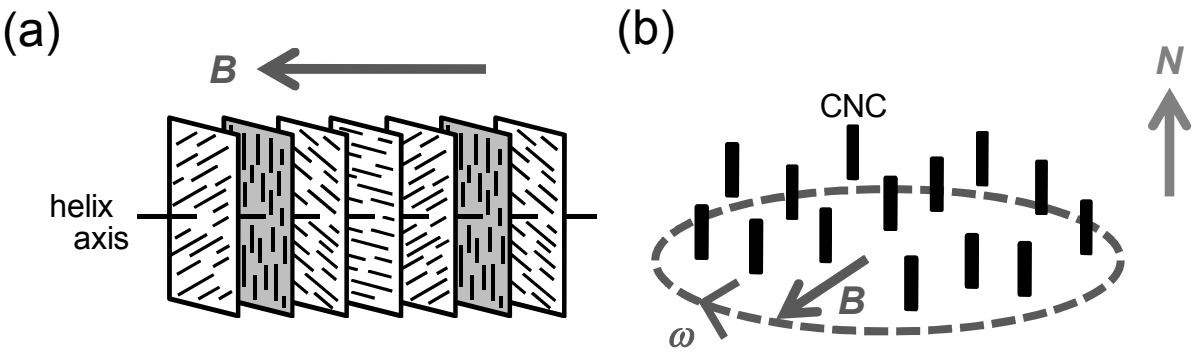

Figure 3-4. Two ideal orientation schemes of mesomorphic CNC assembly: (a) chiral nematic monodomain structure attainable under a static magnetic field; (b) uniaxially oriented nematic state attainable under a rotational magnetic field.

3.3.2. Evaluation of CNC Orientation Distribution by WAXD

Figure 3-5 compiles WAXD photographic data taken for PHEMA-CNC_{aniso}-s and PHEMA-CNC_{aniso}-r composites that were both synthesized in the cylindrical shape. Figure 3-5a–c shows a set of three views (see Figure 3-1c) for the former composite oriented by the static magnetic treatment. In both the normal view and the side-II view, we can find a common WAXD profile characterized by a strong arcing reflection ($2\theta \approx 22.6°$) with the intensity maximum on the meridian. Plainly, this reflection comes from the (200) diffraction of cellulose Iβ.[3,26] In the side-III view (Figure 3-5c), however, there solely appears a random orientation pattern. The crystallographic *c* and *a* axes of cellulose Iβ can be assumed to be parallel and perpendicular, respectively, to the longer axis of CNC, and, therefore, it follows from the WAXD result that the dispersed CNC rods were laid perpendicular to the field vector $\boldsymbol{B}$ ($\|X_{III}$-axis), with no biased directional distribution as a whole in the X_IX_{II}-plane of the composite sample. This supports the attainment of the chiral nematic monodomain structure modeled in Figure 3-4a.

In WAXD measurements for the other composite PHEMA-CNC_{aniso}-r, the normal view provided a random orientation pattern (Figure 3-5d), whereas the side-III view revealed an intense equatorial reflection derived from the cellulose (200) diffraction (Figure 3-5e). This profile in the side-III view was substantially the same as that in the side-II view. From these observations, it can be taken that the longer axes of CNCs were oriented perpendicular to the $X_{II}X_{III}$-plane of $\boldsymbol{B}$ rotation and, accordingly, the nematic state of CNCs modeled in Figure 3-4b was sufficiently fixed into the PHEMA-CNC_{aniso}-r composite.

WAXD measurements were also made for the PHEMA-CNC_{aniso}-e series prepared with application of an elliptical magnetic field, but the obtained orientation patterns of CNC were, in common, similar to that of uniaxial symmetry found for the PHEMA-CNC_{aniso}-r composite. Despite the various modulations of $\boldsymbol{B}$ rotation produced by changing the velocity ratio of ω_1/ω_2 (40/160 or 20/140 rpm/rpm) and the angular range of α (20, 60, or 90°), there occurred no preferred orientation around the longer axis of CNC. This result would be primarily due to the intrinsic anisotropy in the magnetic susceptibility of CNC. Possibly, the anisotropy might be of a high axial symmetry to make only a slight difference in magnitude between the susceptibility components χ_1 and χ_2 involved with shorter axes of CNC, i.e., $|\chi_1| \approx |\chi_2| < |\chi_3|$. However, the three-dimensional alignment of CNC was formerly reported to be fixed into a

UV-cured resin matrix via pretreatment under an elliptical magnetic field, even though the evidence was solely based on a POM observation;[23] viz., a definite biaxial anisotropy was detected for the oriented sample by differentiating polarization colors in three orthogonal directions. The success might be due to the use of an extremely high magnetic field of 12 T, which is practically 2.25 times stronger than the 8 T field in the present study, regarding the torque acting on CNC rods.[27]

Concerning PHEMA-CNC_{iso}-s and PHEMA-CNC_{iso}-r composites prepared from the relevant isotropic suspensions of CNC, any of the WAXD patterns obtained was less indicative of the conceivable magnetic orientation effect. It seemed rather reasonable to judge that CNCs were dispersed nearly at random in those composites. A rapid orientation relaxation concurrent in the magnetic treatment of the suspensions may be responsible for the inherent less attainability of orientation. However, this was not the case for preparations of PHEMA-CNC_{aniso}-s and PHEMA-CNC_{aniso}-r from anisotropic suspensions of CNC, in spite of the never so higher viscosity of the suspensions. Again the authors can deduce that a coherent response as the mesomorphic assembly may be of great significance in the magnetic orientation of CNC suspensions.

A more quantitative estimation of the degree of orientation development of CNC was carried out for several representatives of PHEMA-CNC composites. For this purpose, the authors defined an orthogonal frame O-$x_1x_2x_3$ associated with the susceptibility components $|\chi_i|$ (i = 1, 2, 3) of CNC; here, let the x_3-axis be along the longitudinal axis lying parallel to the c axis of Iβ, then the axes a and b (making $\gamma \approx 97°$) of the monoclinic crystal[26] lie on the x_1x_2-plane. The orientation of the CNC frame O-$x_1x_2x_3$ with respect to the sample coordinate system O-$X_IX_{II}X_{III}$ is specified by three angles, $\phi_{1,\boldsymbol{B}}$, $\phi_{2,\boldsymbol{B}}$, and $\phi_{3,\boldsymbol{B}}$ in Figure 3-6a, and by $\phi_{1,\boldsymbol{N}}$, $\phi_{2,\boldsymbol{N}}$, and $\phi_{3,\boldsymbol{N}}$ in Figure 3-6b. The angles $\phi_{i,\boldsymbol{B}}$ (i = 1, 2, 3) are measured between the susceptibility axes x_i (i = 1, 2, 3) and the principal X_{III}-axis parallel to the applied field $\boldsymbol{B}$, and this situation refers to the PHEMA-CNC_{aniso}-s series. For the PHEMA-CNC_{aniso}-r and -e series, the angles $\phi_{i,\boldsymbol{N}}$ (i = 1, 2, 3) are measured between the respective axes x_i (i = 1, 2, 3) and the X_I-axis parallel to the normal vector $\boldsymbol{N}$ (see Figure 3-1c).

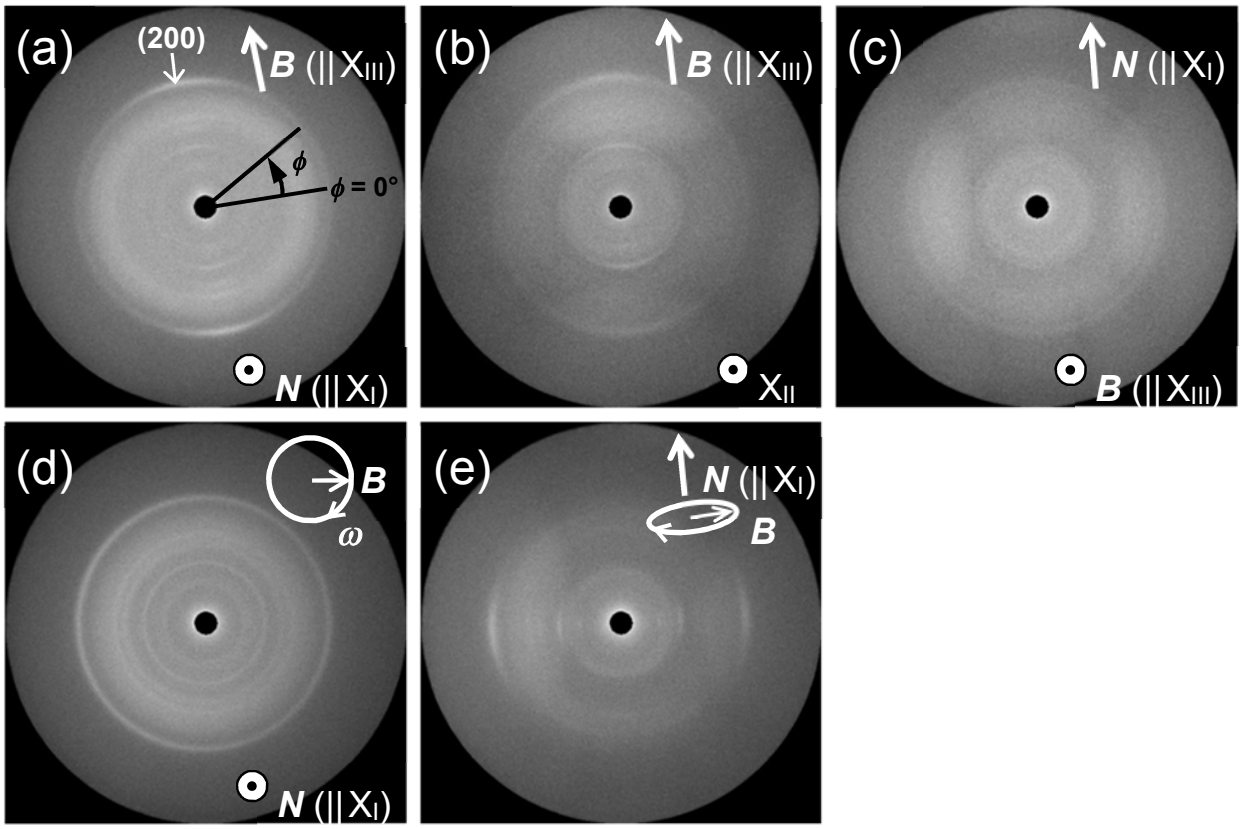

Figure 3-5. WAXD patterns of two polymer composites: (a) normal, (b) side-II, and (c) side-III views for PHEMA-CNC$_{aniso}$-s; (d) normal and (e) side-III views for PHEMA-CNC$_{aniso}$-r. (See Figure 3-1c for definition of the views.)

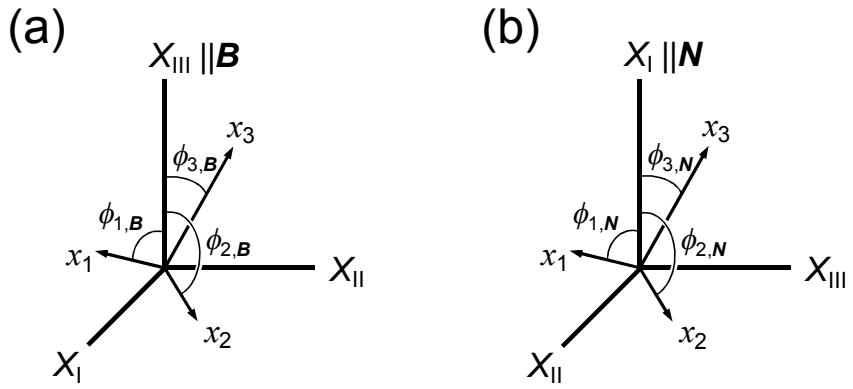

Figure 3-6. Pictorial representations specifying the orientation of a CNC frame O-$x_1x_2x_3$ of magnetic susceptibility with respect to the sample coordinate system O-$X_IX_{II}X_{III}$. The specification (a) is applicable to PHEMA-CNC$_{aniso}$-s with the X_{III}-axis parallel to ***B***, and (b) refers to PHEMA-CNC$_{aniso}$-r and -e with the X_I-axis parallel to ***N***.

In the case of PHEMA-CNC_{aniso}-s, the orientation parameter $f_{i,\boldsymbol{B}}$ of the x_i-axis of CNC is defined as follows,

$$f_{i,\boldsymbol{B}} = (3\langle\cos^2\phi_{i,\boldsymbol{B}}\rangle - 1)/2 \qquad (i = 1, 2, 3) \qquad (1)$$

Generally, this kind of parameter f can vary between −0.5 and 1, that is, $f = 0$ for random orientation of a considered axis, and $f = -0.5$ for perpendicular alignment while $f = 1$ for complete uniaxial orientation.[28] Since the present axes x_1, x_2, and x_3 are mutually right-angled, the following relationships hold.

$$\langle\cos^2\phi_{1,\boldsymbol{B}}\rangle + \langle\cos^2\phi_{2,\boldsymbol{B}}\rangle + \langle\cos^2\phi_{3,\boldsymbol{B}}\rangle = 1 \qquad (2)$$

$$f_{1,\boldsymbol{B}} + f_{2,\boldsymbol{B}} + f_{3,\boldsymbol{B}} = 0 \qquad (3)$$

When the orientation distribution of the x_3-axis ($\|c$) is cylindrically symmetric about the X_{III}-axis and there arises no preferential orientation around the x_3-axis ($|\chi_1| \approx |\chi_2|$), eqs (2) and (3) reduce to the following eqs (4) and (5), respectively, with a statistical relation of $\langle\cos^2\phi_{1,\boldsymbol{B}}\rangle = \langle\cos^2\phi_{2,\boldsymbol{B}}\rangle = \langle\cos^2\phi_{a,\boldsymbol{B}}\rangle$.

$$\langle\cos^2\phi_{3,\boldsymbol{B}}\rangle = 1 - 2\langle\cos^2\phi_{1,\boldsymbol{B}}\rangle = 1 - 2\langle\cos^2\phi_{a,\boldsymbol{B}}\rangle \qquad (4)$$

$$f_{3,\boldsymbol{B}} = -2f_{1,\boldsymbol{B}} = -2f_{a,\boldsymbol{B}} \qquad (5)$$

where $\phi_{a,\boldsymbol{B}}$ is an angle that the crystal axis a makes with the X_{III}-axis and $f_{a,\boldsymbol{B}}$ denotes the orientation parameter of the a axis. The value of $\langle\cos^2\phi_{a,\boldsymbol{B}}\rangle$ and therefore that of $f_{a,\boldsymbol{B}}$ can be estimated from the azimuthal profile of the (200) reflection intensity, according to the conventional integral equation.[28,29]

$$\langle\cos^2\phi_{a,\boldsymbol{B}}\rangle = \frac{\int_0^{\pi} I_{200}(\phi)\cos^2\phi\sin\phi\,\mathrm{d}\phi}{\int_0^{\pi} I_{200}(\phi)\sin\phi\,\mathrm{d}\phi} \qquad (6)$$

where $I_{200}(\phi)$ represents the intensity as a function of the azimuth ϕ for the (200) diffraction of CNC. Then, we can determine the orientation parameters $f_{1,\boldsymbol{B}}$ and $f_{3,\boldsymbol{B}}$ from eq (5).

Figure 3-7a displays the corresponding azimuthal intensity scans for the PHEMA-CNC_{aniso}-s sample used in Figure 3-5a–c. In the intensity profile of normal view, two large peaks are centered at azimuthal angles of 90° and 270°, indicating that the longer axes of CNCs in the polymer matrix tend to be aligned perpendicular to the direction of the static magnetic field. In the azimuthal profile of side-III view, there appears no remarkable peak in accordance with the overall random orientation in the $X_I X_{II}$-plane. Through integral analysis of the former significant data of normal view in terms of eq (6), eventually the authors obtained $f_{1,\boldsymbol{B}} = 0.21$ and $f_{3,\boldsymbol{B}} = -0.42$ for the PHEMA-CNC_{aniso}-s composite. A passable achievement of the perpendicular alignment of the longer axes of CNCs may be

admitted. Additionally, as to the helical axis of chiral nematic organization, we can estimate an attainment of the uniaxial orientation at $f = 0.84$ (= 0.42 × 2).

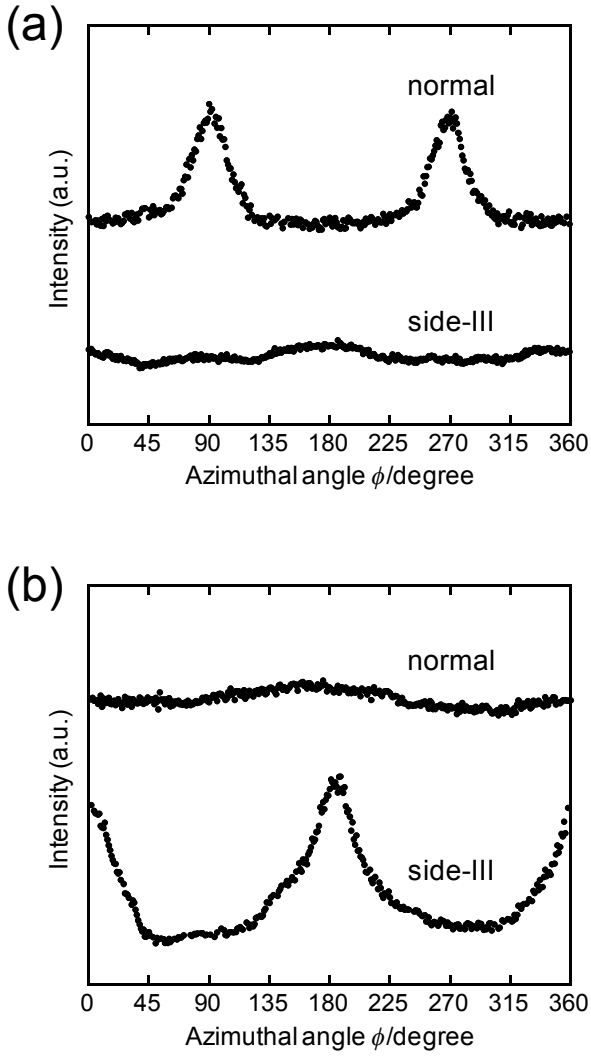

Figure 3-7. Azimuthal intensity profiles of the (200) diffraction of CNC: (a) data for PHEMA-CNC_{aniso}-s; (b) data for PHEMA-CNC_{aniso}-r. These two composites are the same as those used in Figure 3-5. Intensity was scanned in the normal (upper) and side-III (bottom) views.

As regards the case of PHEMA-CNC_{aniso}-r, the orientation parameter $f_{i,N}$ of the x_i-axis of CNC is defined by taking the X_I-axis ($\|\boldsymbol{N}$) as the reference axis. Then, in the same manner as the above, the author can evaluate the parameters $f_{1,N}$ (= $f_{a,N}$) and $f_{3,N}$. In Figure 3-7b, the (200) azimuthal intensity profiles are shown for the PHEMA-CNC_{aniso}-r sample used in Figure 3-5d and e. In the data of side-III view, two major peaks are observed at angular positions of $\phi = 0°$ and 180°, while the scan in the normal view makes no noticeable intensity maximum. These observations confirm that the longer axes of CNCs in the matrix are aligned preferentially perpendicular to the plane of the rotating magnetic field, with the two shorter axes (x_1 and x_2) oriented randomly in the rotation plane. By applying eq (6) to integral analysis of the intensity data of side-III view, the authors obtained $f_{1,N} = -0.30$ and $f_{3,N} = 0.60$ for the PHEMA-CNC_{aniso}-r composite. It may be judged that there is a considerable attainment of the uniaxial alignment of CNC rods to the direction of $\boldsymbol{N}$ in the composite, even though the value $f_{3,N} = 0.60$ is at a remove from the ideal limit of unity. This estimation can be appreciated by comparison with the corresponding data for a similar class, just as shown below.

The orientation parameter $f_{3,N}$ was also determined for the PHEMA-CNC_{aniso}-e series, the values obtained were listed in Table 3-1, together with the data ($f_{3,B}$ and $f_{3,N}$) for the foregoing two samples of PHEMA-CNC_{aniso}-s and PHEMA-CNC_{aniso}-r. In the parentheses following each sample name of the PHEMA-CNC_{aniso}-e series, an average velocity of the modulated rotation of $\boldsymbol{B}$ is indicated. The authors find that the parameter $f_{3,N}$ increases with an increase in the average ω from 80 to 146 rpm in the same series and ultimately assumes the highest value of 0.60 in the PHEMA-CNC_{aniso}-r composite prepared under the constantly rotating field with a single velocity of 150 rpm. Further quantification of $f_{3,N}$ was made in the same way for a few samples of PHEMA-CNC_{iso}-r prepared from isotropic CNC suspensions. As a result, the author got a value of $f_{3,N}$ approximating 0.1 and over, with a great uncertainty depending on the correction of WAXD intensity by subtracting the background.

Table 3-1. Evaluations of Orientation Parameters of the Longitudinal Axis of CNC for PHEMA-CNC_{aniso} Composites Prepared Under Various Magnetic Fields

Sample	Orientation parameter	
	$f_{3,\boldsymbol{B}}$	$f_{3,\boldsymbol{N}}$
PHEMA-CNC_{aniso}-s	−0.42	-
PHEMA-CNC_{aniso}-r (ω = 150 rpm)[a]	-	0.60
PHEMA-CNC_{aniso}-e-20/140-90 (ω = 80 rpm)[a]	-	0.41
PHEMA-CNC_{aniso}-e-40/160-90 (ω = 100 rpm)[a]	-	0.48
PHEMA-CNC_{aniso}-e-40/160-20 (ω = 146 rpm)[a]	-	0.52

[a] Average velocity of the rotation of ***B***-field.

Concerning polymer-CNC (or chitin nanocryastal (ChtNC)) composites prepared by other orientation techniques, a limited number of studies have focused on such a quantitative estimation of the degree of orientation (or order parameter) of the dispersed nanocrystals. Belamie et al.[30] fixed shear-alignment states of α-ChtNC chiral nematic suspensions into polymer matrices by UV-induced polymerization of acrylamide precursors added to the medium; then, the research group determined a high order parameter of 0.8 for the selected samples by small-angle X-ray scattering. In comparison with this situation, the orientation state of $f_{3,\boldsymbol{N}}$ = 0.60 estimated for the PHEMA-CNC_{aniso}-r composite is apparently lower, whereas the orientation state of f = 0.84 (helix axis) and $f_{3,\boldsymbol{B}}$ = −0.42 (CNC axis) in the PHEMA-CNC_{aniso}-s composite, realized under a unidirectional magnetic stimulus, may be in a parallel or rather higher level. Meanwhile, Boltoeva et al.[31] attempted to carry over electric field-induced alignments of similar α-ChtNC suspensions into nanocomoposites with silica via sol-gel conversion of siloxane oligomers mixed therein; however, a low order parameter (~0.3) was only attained.

3.3.3. Dynamic Mechanical Analysis of Composites

DMA results obtained in tension mode for two strips cut from the same film of PHEMA-CNC_{aniso}-s are shown in Figure 3-8; the values of E' (part a) and E'' (part b) are plotted as a function of temperature to be compared with the corresponding data for reference samples of PHEMA and PHEMA-CNC_{aniso} prepared under no magnetic field. The two strips of PHEMA-CNC_{aniso}-s are distinguished from each other by additional notations $\parallel$ and $\perp$. As depicted in Figure 3-9a, these notations indicate whether the applied tensile stress was parallel ($\parallel$) or perpendicular ($\perp$) to the direction of the magnetic field that had been employed in the initial film preparation.

With regard to the PHEMA and PHEMA-CNC_{aniso} samples as reference, the present DMA measurements well reproduced their thermomechanical characteristics revealed in the preceding chapter.[24] Namely, the PHEMA film exhibited a principal dispersion centering ~110 °C and a secondary one as a broad shoulder locating around 45 °C in the E'' versus temperature curve; the former dispersion corresponds to the glass transition and the latter refers to a local chain relaxation of this methacrylate polymer. Looking over the data for the PHEMA-CNC_{aniso} composite, we can readily see several significant changes in the thermomechanical property of PHEMA caused by the locking-in of the CNC assembly; for instance, there arises an elevation in the glassy modulus E' of PHEMA as well as a drastic suppression of the E'-drop in the glass transition region of this polymer, each observation demonstrating an effective reinforcement action of the CNC component on the polymer matrix. The re-rise of the composite modulus, observed in a temperature range of ca. 150–190 °C, is a secondary effect due to cross-linking of PHEMA catalyzed by the acidic CNC filler.[24]

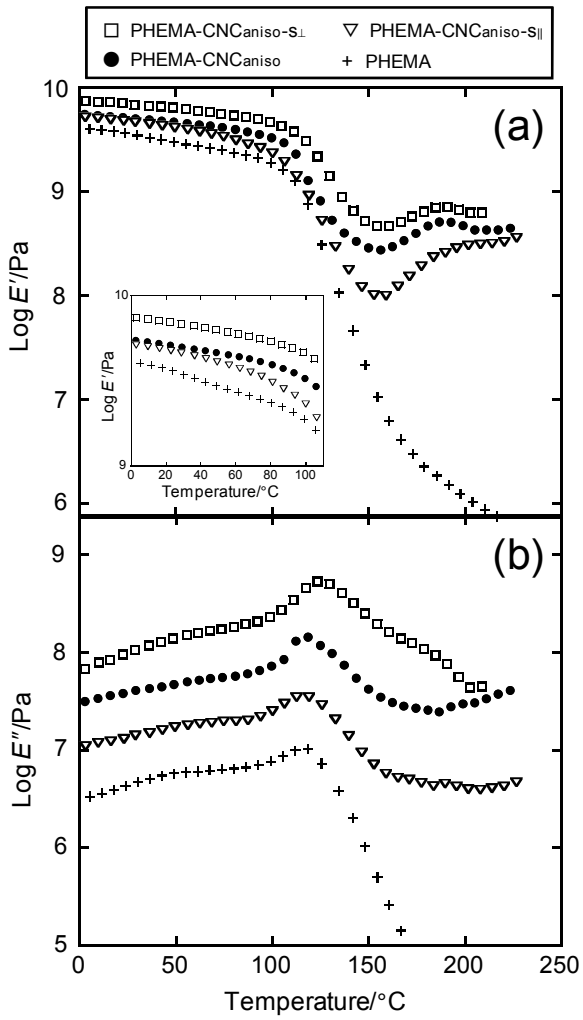

Figure 3-8. Temperature dependence of the storage modulus (E') and loss modulus (E''), measured in tension mode for film samples of PHEMA-CNC_{aniso}-s, and PHEMA and PHEMA-CNC_{aniso} references: (a) E' data for each sample, and an enlarged plot of the glass-state modulus E' (inset); (b) E'' data plotted by displaying by ~0.5 log unit in the ordinate. As to the PHEMA-CNC_{aniso}-s composite, two rectangular strips distinguished from each other by notations || and ⊥ (see Figure 3-9a) were used for the tension-mode DMA measurements.

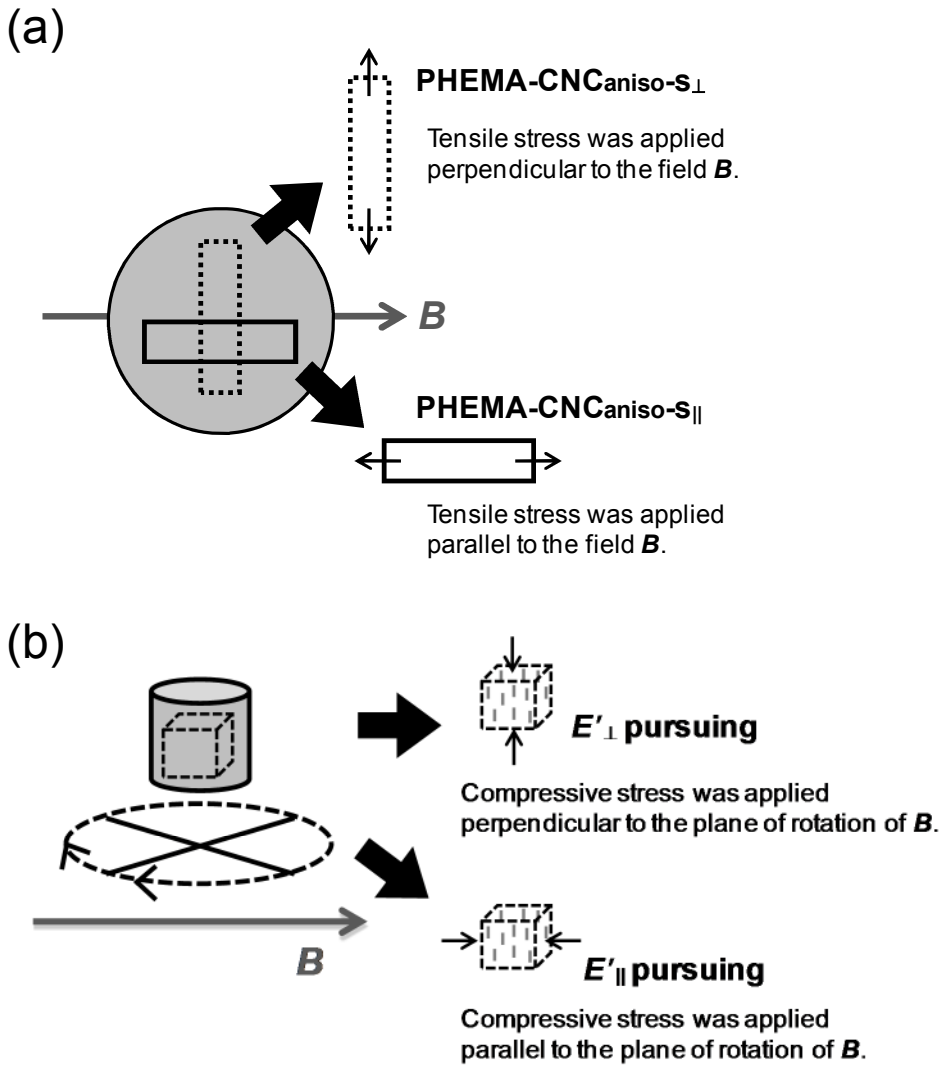

Figure 3-9. Schematic illustrations of PHEMA-CNC samples used for DMA measurements: (a) film strips of PHEMA-CNC_{aniso}-s subjected to the measurements in tension mode; (b) cuboid specimens of PHEMA-CNC composites subjected to the measurements in compression mode.

The major concern in the present DMA study is to find some effects of the orientation distribution of CNC rods on the mechanical property of the PHEMA-CNC composites magneto-treated variously. As is evident in Figure 3-8a, both of the two strips of PHEMA-CNC_{aniso}-s imparted substantially the same reinforcing effect of the CNC incorporation as that described for the reference PHEMA-CNC_{aniso}. However, the modulus E' of PHEMA-CNC_{aniso}-$s_{\perp}$ was usually situated higher relative to that of PHEMA-CNC_{aniso}-$s_{\parallel}$, and the reference PHEMA-CNC_{aniso} retained an intermediate modulus between the former two. Moreover, the respective E'' plots for these three samples (Figure 3-8b) produced a peak maximum (associated with T_g) at different temperatures of 126 °C (PHEMA-CNC_{aniso}-$s_{\perp}$), 115 °C (PHEMA-CNC_{aniso}-$s_{\parallel}$), and 120 °C (PHEMA-CNC_{aniso}); this careful reading may have disclosed a delicate difference of the effectiveness in elevating the T_g (112 °C) of PHEMA between the three film samples, all containing ~12 wt % CNCs. Plainly the improvement in the thermomechanical performance was pronounced in the order of PHEMA-CNC_{aniso}-$s_{\parallel}$ < PHEMA-CNC_{aniso} < PHEMA-CNC_{aniso}-$s_{\perp}$. This rank order may be correlated to the practical content of CNC rods pointing to the tensile stress direction. In the PHEMA-CNC_{aniso}-$s_{\perp}$ sample, virtually a half part of the dispersed CNCs assumes the parallel orientation of their longitudinal axis toward the tensile direction ($\perp\boldsymbol{B}$) (see Figure 3-4a), if the individual CNCs are treated as a vector quantity. In the PHEMA-CNC_{aniso}-$s_{\parallel}$ sample, the longer axes of all dispersed CNCs are basically aligned perpendicular to the tensile direction, which should make comparatively less contribution to the mechanical reinforcing effect. In the PHEMA-CNC_{aniso} reference, by extension of the simple vectorial treatment, ~33 % of the CNC component would contribute to the effect of reinforcing the polymer matrix; for the reference composite is optically birefringent, but mechanically isotropic when viewed macroscopically.

To further demonstrate the magnetic orientation effect of CNC on the mechanical property of PHEMA-CNC composites, DMA measurements were conducted in compression mode for their respective cuboid specimens. Figure 3-9b depicts two different manners of sample setting relative to the compressive direction, whereby the moduli $E'_{\parallel}$ and $E'_{\perp}$ of the considered composite are defined in relation to the initially applied magnetic field. In calculation of the differential modulus $\Delta E' = E'_{\perp} - E'_{\parallel}$, values of the two compressive moduli were corrected by subtracting the corresponding values for PHEMA control; habitually, $E'_{\parallel}$ was slightly higher than $E'_{\perp}$ in the reference cuboids, which probably comes from the

imperceptible gradient in the solidification rate of HEMA along the depth of the original cylindrical sample. Important results of the DMA measurements are collected in Figure 3-10.

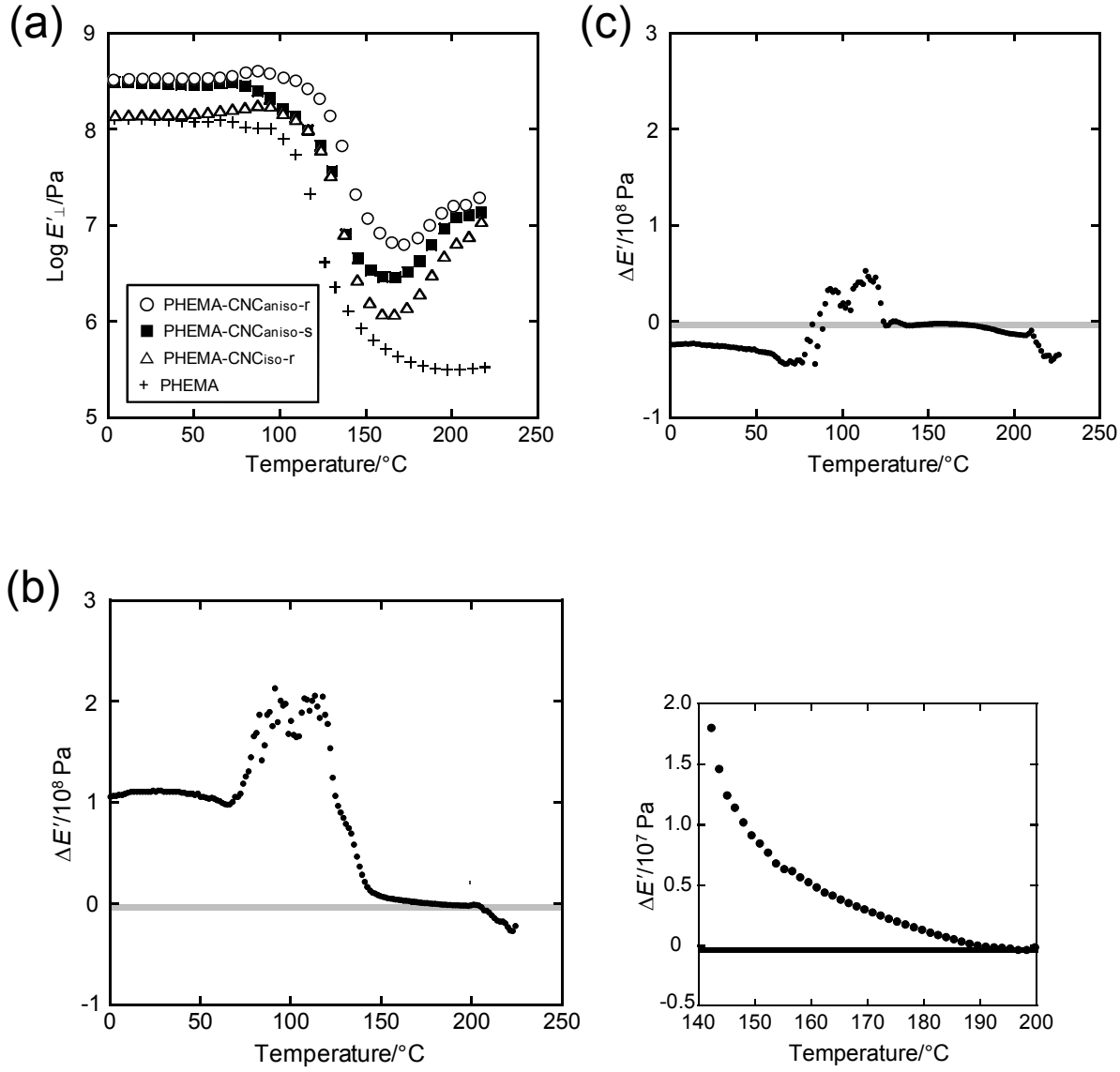

Figure 3-10. Temperature dependence of the modulus $E'_{\perp}$ and differential $\Delta E'$ ($= E'_{\perp} - E'_{\parallel}$), measured in compression mode for cuboid samples of PHEMA and various PHEMA-CNC composites: (a) $E'_{\perp}$ data for PHEMA-CNC_{aniso}-r, PHEMA-CNC_{iso}-r, PHEMA-CNC_{aniso}-s, and PHEMA (reference); (b) $\Delta E'$ data for PHEMA-CNC_{aniso}-r; (c) $\Delta E'$ data for PHEMA-CNC_{iso}-r. Two compressive conditions for obtaining $E'_{\perp}$ and $E'_{\parallel}$ are depicted in Figure 3-9b.

Figure 3-10a displays $E'_{\perp}$ data obtained in the compressive oscillations perpendicular to the plane on which the ***B***-field was laid, for cuboids of PHEMA (reference), PHEMA-CNC_{aniso}-r, PHEMA-CNC_{iso}-r, and PHEMA-CNC_{aniso}-s. In comparison between four composites including a PHEMA-CNC_{aniso} cubic reference (data not shown for this), the magnitude of the compressive modulus was ranked in the order of PHEMA-CNC_{iso}-r < PHEMA-CNC_{aniso} < PHEMA-CNC_{aniso}-s < PHEMA-CNC_{aniso}-r. This order well reflects the differences in aggregation and orientation states of the dispersed CNC component between the composites. First, it seems reasonable that the PHEMA-CNC_{aniso}-r composite exhibited the highest modulus in this compression mode (upper in Figure 3-9b), in view of the attainment of the high degree of uniaxial orientation of CNCs characterized by $f_{3,N}$ = 0.60 ($\langle\cos^2\phi_{3,N}\rangle$ = 0.74). Secondly, the superiority of the PHEMA-CNC_{aniso}-s sample to the PHEMA-CNC_{aniso} reference can be interpreted as due to the more uniform chiral nematic planar arrangement of CNCs in the former composite ($f_{3,B}$ = −0.42). Finally, the last place of the PHEMA-CNC_{iso}-r composite is satisfactorily explained by the lower CNC concentration (leading to less mesomorphic order) as well as by the nearly isotropic distribution of CNCs in the polymer matrix.

In Figure 3-10b and c, the authors compared two plots of the differential $\Delta E'$ (= $E'_{\perp} - E'_{\parallel}$) versus temperature data measured for cuboid samples of PHEMA-CNC_{aniso}-r and PHEMA-CNC_{iso}-r. In the plot for the latter (Figure 3-10c), in perspective, $\Delta E'$ is situated around 0 over the whole temperature range explored, indicating that the mechanical anisotropy is poor in the PHEMA-CNC_{iso}-r composite. This is in consistence with the nearly random orientation of CNCs, which was revealed by the microscopy and WAXD analyses for this class of PHEMA-CNC composites. In contrast, the other class PHEMA-CNC_{aniso}-r definitely exhibited the mechanical anisotropy in the DMA data (Figure 3-10b); the modulus $E'_{\perp}$ was easily higher than $E'_{\parallel}$ at temperatures of ≤150 °C and this anisotropy was actually detected up to ~195 °C in an enlarged scale of the $\Delta E'$ plot (see the example of magnification for a range of 140–200 °C in Figure 3-10b). A comparable anisotropy in compressive modulus was also observed for the PHEMA-CNC_{aniso}-s composite retaining a uniform chiral nematic arrangement. Regarding these plots of $\Delta E'$ versus temperature, lastly, we should remark that a more or less pulsating peak signal appeared in a range of ca. 80–130 °C, which is attributable to occurrence of the cross-linking of PHEMA molecules mediated by the acidic CNC filler.[24] The largest positive contribution of this effect to $\Delta E'$ (therefore to $E'_{\perp} > E'_{\parallel}$)

was observed for the PHEMA-CNC_{aniso}-r composite (Figure 3-10b), implying that the uniaxial orientation of CNCs efficiently promotes the cross-linking between PHEMA chains and partly between PHEMA and CNC as well. In connection with this, the PHEMA chains might have been locally ordered parallel to the neighboring CNCs, already in the polymerization process of HEMA monomer.

References

(1) Habibi, Y.; Lucia, L. A.; Rojas, O. J. *Chem. Rev.* **2010**, *110*, 3479–3500.

(2) Klemm, D.; Kramer, F.; Moritz, S.; Lindström, T.; Ankerfors, M.; Gray, D. G.; Dorris, A. *Angew. Chem. Int. Ed.* **2011**, *50*, 5438–5466.

(3) Moon, R. J.; Martini, A.; Nairn, J.; Simonsen, J.; Youngblood, J. *Chem. Soc. Rev.* **2011**, *40*, 3941–3994.

(4) Eichhorn, S. J. *Soft Matter* **2011**, *7*, 303–315.

(5) Favier, V.; Chanzy, H.; Cavaillé, J. Y. *Macromolecules* **1995**, *28*, 6365–6367.

(6) Favier, V.; Canova, G. R.; Cavaillé, J. Y.; Chanzy, H.; Dufresne, A.; Gauthier, C. *Polym. Adv. Technol.* **1995**, *6*, 351–355.

(7) Marchessault, R. H.; Morehead, F. F.; Walter, N. M. *Nature* **1959**, *184*, 632–633.

(8) Revol, J. -F.; Bradford, H.; Giasson, J.; Marchessault, R. H.; Gray, D. G. *Int. J. Biol. Macromol.* **1992**, *14*, 170–172.

(9) Dong, X. M.; Kimura, T.; Revol, J. -F.; Gray, D. G. *Langmuir* **1996**, *12*, 2076–2082.

(10) Dong, X. M.; Revol, J. -F.; Gray, D. G. *Cellulose* **1998**, *5*, 19–32.

(11) Gray, D. G. *Carbohydr. Polym.* **1994**, *25*, 277–284.

(12) Ureña-Benavides, E. E.; Brown, P. J.; Kitchens, C. L. *Langmuir* **2010**, *26*, 14263–14270.

(13) Uddin, A. J.; Araki, J.; Gotoh, Y. *Biomacromolecules* **2011**, *12*, 617–624.

(14) Timbrell, V. *J. Appl. Phys.* **1972**, *43*, 4839–4820.

(15) Sugiyama, J.; Chanzy, H.; Maret, G. *Macromolecules* **1992**, *25*, 4232–4234.

(16) Kimura, T.; Ago, H.; Tobita, M.; Ohshima, S.; Kyotani, M.; Yumura, M. *Adv. Mater.* **2002**, *14*, 1380–1383.

(17) Kvien, I.; Oksman, K. *Appl. Phys. A: Mater. Sci. Process.* **2007**, *87*, 641–643.

(18) Pullawan, T.; Wilkinson, A. N.; Eichhorn, S. J. *Biomacromolecules* **2012**, *13*, 2528–2536.

(19) Revol, J. -F.; Godbout, L.; Dong, X. M.; Gray, D. G.; Chanzy, H.; Maret, G. *Liq. Cryst.* **1994**, *16*, 127–134.

(20) Kimura, T.; Yoshino, M.; Yamane, T.; Yamato, M.; Tobita, M. *Langmuir* **2004**, *20*, 5669–5672.

(21) Kimura, F.; Kimura, T.; Tamura, M.; Hirai, A.; Ikuno, M.; Horii, F. *Langmuir* **2005**, *21*,

2034–2037.

(22) Kimura, T.; Kimura, F.; Yoshino, M. *Langmuir* **2006**, *22*, 3464–3466.

(23) Kimura, F.; Kimura, T. *J. Phys.: Conf. Ser.* **2009**, *156*, 012002.

(24) Tatsumi, M.; Teramoto, Y.; Nishio, Y. *Biomacromolecules* **2012**, *13*, 1584–1591.

(25) Majoinen, J.; Kontturi, E.; Ikkala, O.; Gray, D. G. *Cellulose* **2012**, *19*, 1599–1605.

(26) Sugiyama, J.; Vuong, R.; Chanzy, H. *Macromolecules* **1991**, *24*, 4168–4175.

(27) Kimura, T. *Polym. J.* **2003**, *35*, 823–843.

(28) Stein, R. S. *J. Polym. Sci.* **1958**, *31*, 327–334.

(29) Wilkes, G. L. *Adv. Polym. Sci.* **1971**, *8*, 91–136.

(30) Belamie, E.; Davidson, P.; Giraud-Guille, M. M. *J. Phys. Chem. B* **2004**, *108*, 14991–15000.

(31) Boltoeva, M. Y.; Dozov, I.; Davidson, P.; Antonova, K.; Cardoso, L.; Alonso, B.; Belamie, E. *Langmuir* **2013**, *29*, 8208–8212.

Chapter 4
Different Orientation Patterns of Cellulose Nanocrystal Films Prepared from Aqueous Suspensions by Shearing under Evaporation

4.1. Introduction

Fragmented microfibrils of cellulose, commonly termed cellulose nanocrystals (CNCs), are highly crystalline rod-like particles obtained by acid hydrolysis of native cellulose fibers.[1,2] Particularly, CNCs prepared by the hydrolysis with sulfuric acid show an adequate dispersibility in water due to the negative charge of their sulfated surface. The resulting colloidal CNC suspension manifests a unique character to form a self-ordering mesoscopic structure via spontaneous phase separation[2–5]; that is, above a critical concentration of CNC (typically 3–5 wt % for cotton-derived CNCs), the visually homogeneous suspension separates into an upper random phase (isotropic) and a lower ordered phase (anisotropic) in the course of quiescent standing. In the anisotropic phase, CNCs as mesogen form a chiral nematic organization.

In recent years, there has been increasing interest in CNCs as a promising key component to design new materials exhibiting optical functionality or mechanical high-performance, in context of the CNC's fascinations such as the nanoscale dimension with a high aspect ratio and the inherent high stiffness.[6–8] For instance, CNCs can be ideal fillers for high-performance polymer nanocomposites, and, in fact, there have been many reports on the excellent filler effects of CNCs reinforcing various polymer matrices.[9–11]

In conditioning of the optical, mechanical, or thermo-mechanical properties of CNC-containing materials, the orientation control of CNCs is of great importance. Various attempts have been made to align CNCs in aqueous media and fix the orientation state in the dried films or polymer composites, for the purpose of making their properties anisotropic and upgraded. According to the situations, different methods were adopted to align CNCs; for example, CNCs were aligned in the suspensions by deformation of shearing[12] or drawing[13–15], and also by a non-contact technique of applying magnetic fields[16–18].

In this chapter, the authors successfully demonstrated the investment of a clear mechanical anisotropy in polymer composites with CNC[18]; where the orientation control of

CNC fillers was made using a magnetic alignment system. Briefly, the composites were prepared from cotton CNC/aqueous 2-hydroxyethyl methacrylate (HEMA) suspensions, via magnetic field application to the suspensions followed by polymerization of the monomer HEMA in the solvent. Applying a magnetic field (8 T) of static (s) or rotational (r) type to each mesophase of the phase-separated CNC suspensions resulted in fabrication of a composite of CNC/poly(2-hydroxyethyl methacrylate) (PHEMA) designated PHEMA-CNC_{aniso}-s or PHEMA-CNC_{aniso}-r. A uniform structure of chiral nematic monodomain of CNC was fixed into PHEMA-CNC_{aniso}-s (see Fig. 4-6c), and, in PHEMA-CNC_{aniso}-r, CNC particles were distributed with their respective longer axes aligned normal to the plane of the field rotation (Fig. 4-6d).

In this chapter, the authors turned attention to a mechanical way to make a highly oriented CNC film from suspension under shear flow; it is just the way proposed by Nishiyama et al.[12]. They used a CNC sample isolated from the cell wall of a green alga, the particle size being ~40 nm in diameter and ~4 μm in length (aspect ratio ≈ 100). An aqueous suspension of the sulfuric acid-treated CNC was prepared at 1 % in a glass vial, and this vial was kept horizontal and rotated around its center at 500 rpm. After 12 h rotation, a gel-like layer formed on the inner surface of the container was washed and dried into a solid film of CNC. The CNCs in the film were highly oriented in the direction of the applied shear flow. Consulting this Nishiyama's method, the authors prepared dry films of cotton-derived CNC from the aqueous suspensions by a similar shearing method, to see the alignment state of CNC attainable therein. Special care was exercised to pH condition of the starting suspension to be sheared. The obtained CNC films were characterized by optical and electron microscopy observations and wide-angle X-ray diffraction (WAXD) measurements. On the pattern and degree of CNC orientation, a comparative survey was made between the CNC films and the composites of PHEMA-CNC_{aniso}-s and PHEMA-CNC_{aniso}-r.

4.2. Experimental Section

4.2.1. Preparation of CNC

The procedure for preparing the CNC used in this work was essentially the same as that described in the preceding chapter[19]. In brief, CNC particles were isolated from cotton cellulose powder (Whatman, CF11) by acid hydrolysis with 65 wt % sulfuric acid, with mechanical stirring at 70 °C for 15 min. After a dilution and centrifugation process, the fluid dispersion of CNC was dialyzed in distilled water for an adequate time period, and concentrated appropriately. The particle dimensions of CNC are 95 nm in length and 9 nm in diameter on average; the axial ratio is around 10. Surface sulfur content of the CNC particles (well refined) approximated ~1.1 wt %, when determined by alkali titration.

4.2.2. Preparation of CNC Films by Shearing Method

A concentrated CNC/water suspension (CNC = ~25 wt %) mentioned above was diluted and homogenized, and a suspension sample of 4 wt % CNC (Suspension A) was prepared at pH = 2.0. Subsequently, half of this suspension was separately neutralized with addition of a small quantity of sodium hydroxide aqueous solution, and a 3.4 wt % CNC suspension (Suspension N) was prepared at pH = 6.7. They were about the isotropic–biphasic critical concentration, but used in the non-separating mixture before the phase separation. The suspensions of 4.9 mL (the former A) and 5.4 mL (the latter N) were each put into a 20 mL glass vial of 25 mm in inner diameter. As illustrated in Figure 4-1, the vial was kept horizontal, and rotated around its center at 700 rpm in an air blower of 40 °C; the tangential direction of the rotation is taken to correspond to the shear direction (SD). The shear rate applied was roughly ~580 s^{-1} and ~530 s^{-1} for Suspensions A and N, respectively, by estimating the thickness (1.5–1.7 mm) of the respective fluids spread over the inside wall at an earlier stage of the rotation. About 20 h later, a dry film of CNC was formed on the inner surface of the glass wall. The film samples thus obtained were encoded by the pH value of the starting suspension: CNC-2.0 and CNC-6.7 from Suspensions A and N, respectively.

Substantially the same preparation of CNC films was repeated to confirm reproducibility of the orientation patterns observed for CNC-2.0 and CNC-6.7 by WAXD measurements, etc.

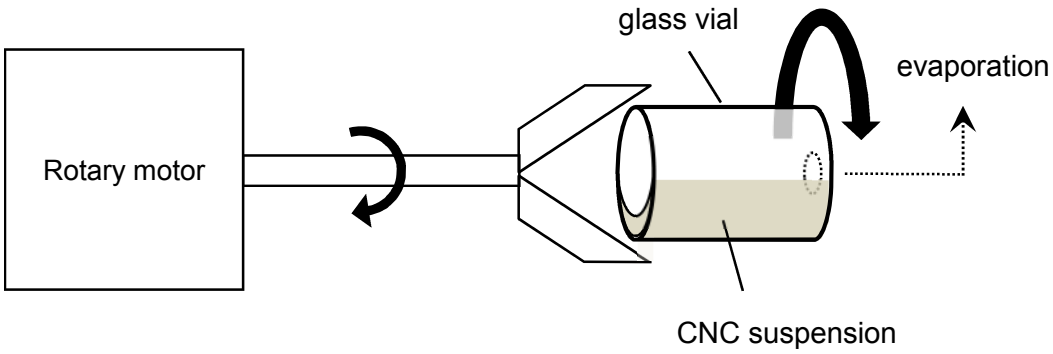

Figure 4-1. Schematic illustration of preparation of oriented CNC films from aqueous suspension by shearing under evaporation. The sample container (glass vial) was rotated at 700 rpm.

4.2.3. Measurements

Optical characterization of CNC films was made under a polarized optical microscope (POM), Olympus BX60F5. The film specimens were also observed by using a field emission scanning electron microscope (FE-SEM), Hitachi S-4800; they were sputter-coated with Pt before the observation.

WAXD measurements were made using a MAC Science Dip 2000 diffractometer equipped with an MXP18HF22 rotating anode generator. The measuring conditions were as follows: voltage and current of operation, 45 kV and 84 mA; X-ray wavelength, 0.154 nm (Ni-filtered CuKα); collimator size, 0.90 mm; camera distance, 150 mm; exposure time, 1800 s. X-ray beam was irradiated perpendicular to the surface of the films.

4.3. Results and Discussion

4.3.1. Microscopic Observations of CNC Films

Generally translucent films of CNC were obtained by the shearing method in either of the pH conditions, as the appearance is exemplified in Figure 4-2a. The CNC films were removed from the vial as several pieces, each showing a habit of curving along SD in some degree. The film thickness varied with location, e.g., from 0.1 to 0.5 mm in CNC-2.0, and the average value approximated 0.2 mm for CNC-2.0 and 0.35 mm for CNC-6.7; thicker parts of the films were, more or less, glossy and brownish. The inclination from the horizontal of the rotation axis in the process of shearing would be partly responsible for the variation and irregularity in film thickness. In the following microscopic and X-ray measurements, film specimens of 0.2–0.25 mm thick were mainly used.

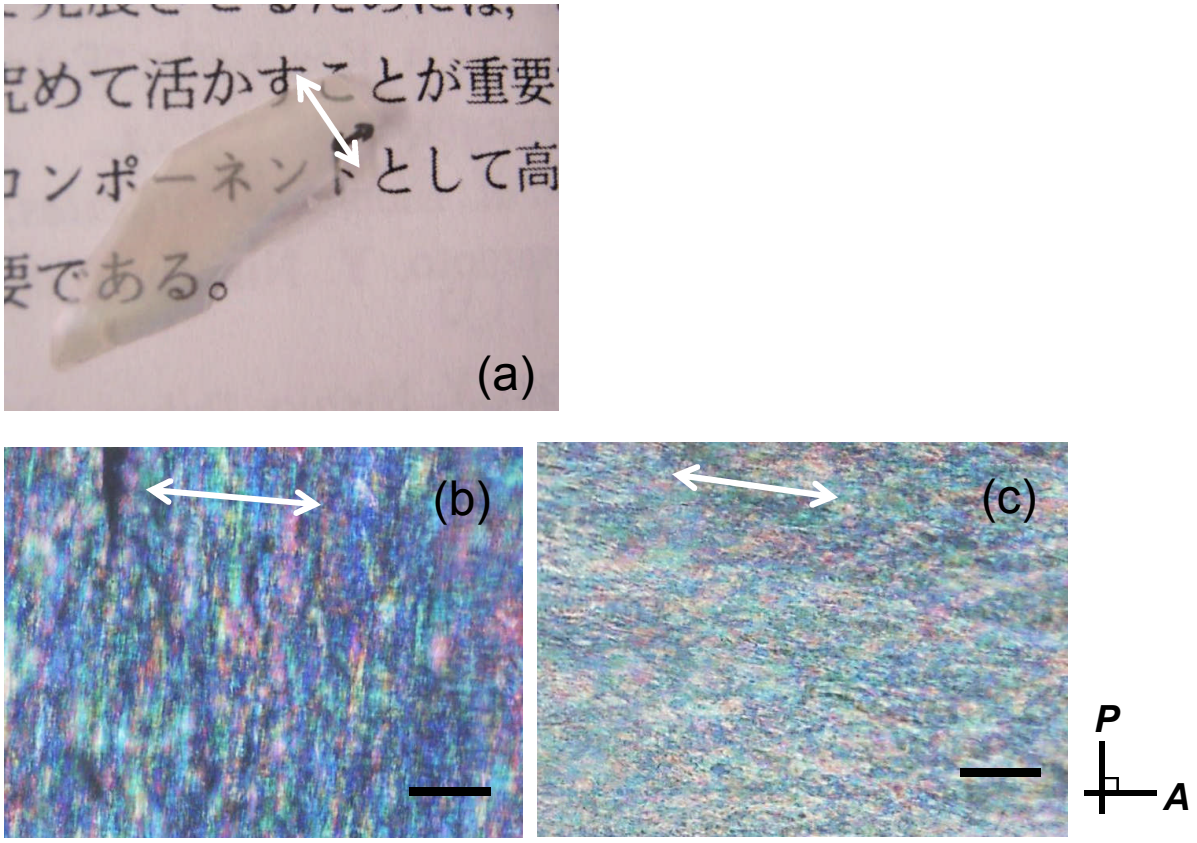

Figure 4-2. Visual appearance of a strip of CNC-2.0 (panel a), and polarized optical micrographs of CNC-2.0 (panel b) and CNC-6.7 (panel c) printed with a scale bar of 50 μm. White arrows indicate the shear direction (SD) of films.

Figure 4-2b and c show POM photographs of CNC-2.0 and CNC-6.7 samples, respectively; both photographs were taken by setting each sample nearly at an orthogonal position (SD || ***P*** or ***A***) on the stage. The field of view was then considerably dark as a whole, when compared with the bright field in a diagonal setting, but the perfect extinction scarcely took place. Rather, as seen in both data, interference colors were still discernible and mingled with fine dark lines (more readily visible in Fig. 4-2b). This observation may be interpreted as being due to the essentially laminated fashion of the films, which were processed via repeated shear deformations of CNC suspensions while drying. The privileged optical axis of the respective oriented films was generally perpendicular to SD (CNC-2.0) and parallel to SD (CNC-6.7).

Selected data of FE-SEM observations for CNC films are given in Figure 4-3. In the observations, the authors found numerous fibrous entities (assimilation of CNCs) aligned mostly in good order in both CNC-2.0 and CNC-6.7 films. While the CNC alignment was preferentially parallel to SD in CNC-6.7 (Fig. 4-3c), the opposite, transverse alignment prevailed in CNC-2.0 (Fig. 4-3a). In the CNC-2.0 film, there also appeared a somewhat different fashion of fibrils' alignment in places; they formed a V- or U-like trajectory of orientation, as shown in Figure 4-3b. This morphology is apparently like the banded structure characteristic of sheared-deformed polymer liquid crystals[20,21], but, rather, it may be regarded as the trace of a helical arrangement of CNCs[19,22]; viz., the chiral nematic structure could develop in the process of condensation of the sheared suspension and partly remain in the dry sample, as discussed below. Another attention should be paid to the fact that no trace of such a mesomorphic organization was observed in the CNC-6.7 film.

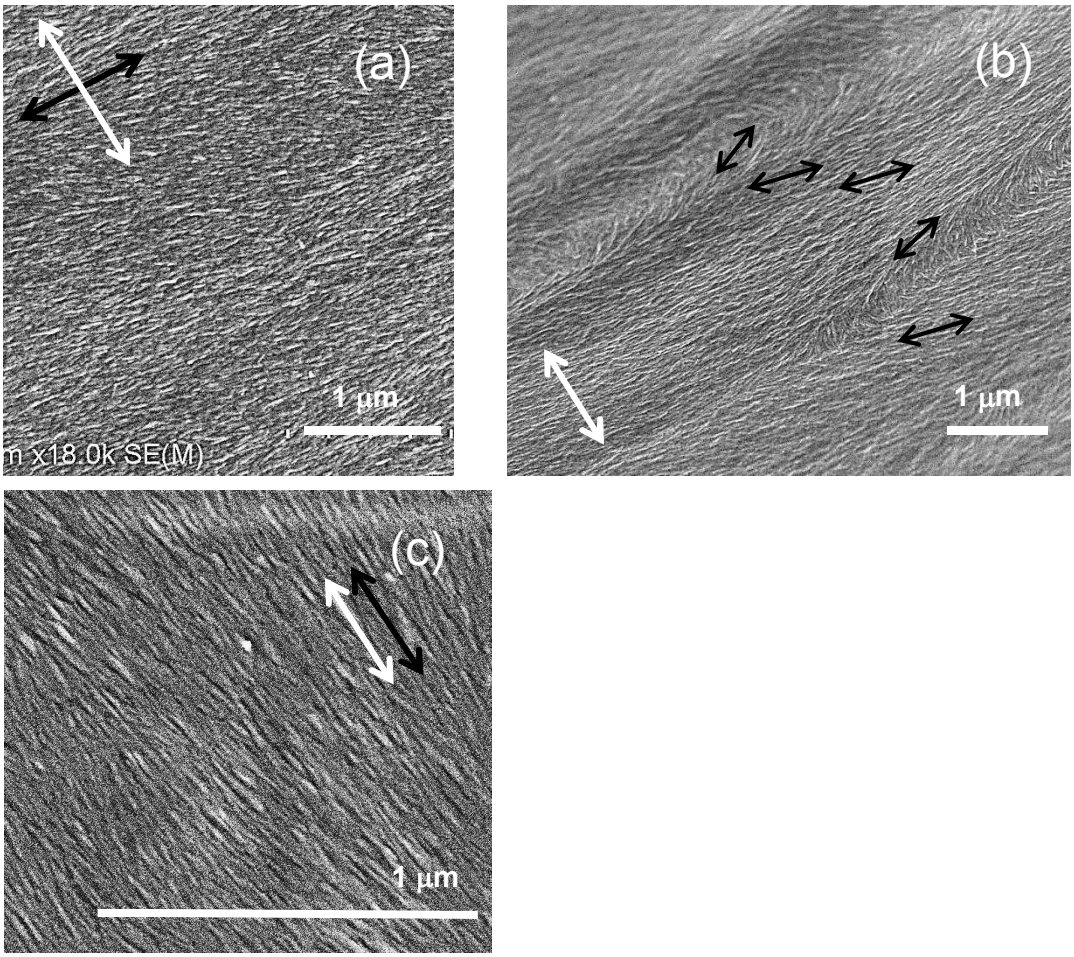

Figure 4-3. FE-SEM images of shear-deformed CNC films: (a) and (b) data for CNC-2.0; (c) data for CNC-6.7. White arrows indicate SD, and black arrows guide the alignment direction of fibrous entities (assimilation of CNCs) to the eye.

4.3.2. CNC Orientation Distribution Revealed by WAXD

Figure 4-4a and b illustrate WAXD photographic data taken for films of CNC-2.0 and CNC-6.7, respectively; SDs of the two samples were both set horizontal, namely, parallel to the equator of the respective WAXD diagrams. The diffraction profiles of both data were characterized by cellulose Iβ of a monoclinic crystal form[23]. This is instantiated by observation of the (200), (110), and ($1\bar{1}0$) diffractions at $2\theta = 22.6°$, 16.6°, and 14.6°, respectively, each appearing as twined reflection arcs across the equator (Fig. 4-4a) or the meridian (Fig. 4-4b). Figure 4-5 displays the azimuthal scanning of the (200) diffraction intensity for the two samples used in Figure 4-4. In Figure 4-5a for CNC-2.0, we find two large peaks centered at azimuthal angles of 0° and 180°; this definitely indicates that the *c*-axis of CNC and therefore the longitudinal axis tends to be aligned perpendicular to SD of the film. In Figure 4-5b for CNC-6.7, two peaks are located with the intensity maximum at azimuthal angles of 90° and 270°; hence, the longer axes of CNCs are aligned preferentially parallel to SD of the film. These WAXD results correspond to the FE-SEM observations of fibrillar alignment that well distinguished between the two CNC films.

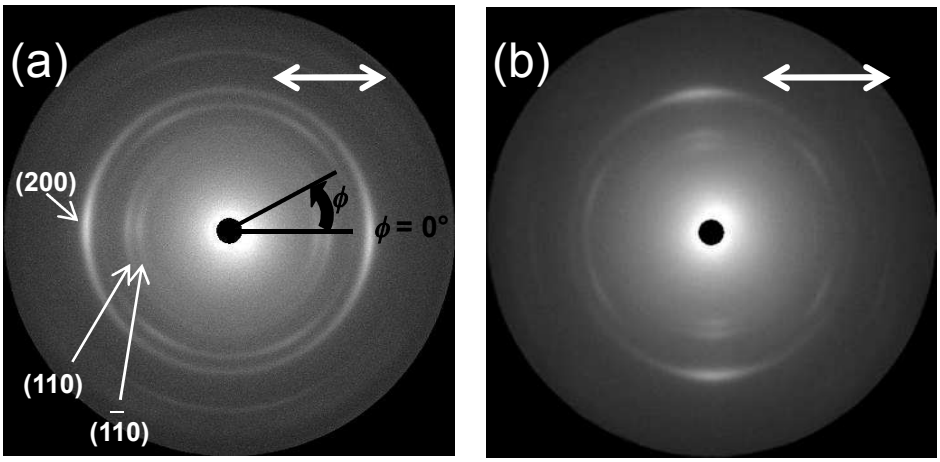

Figure 4-4. WAXD patterns of shear-deformed CNC films: (a) data for CNC-2.0; (b) data for CNC-6.7. White arrows indicate SD of the film specimens.

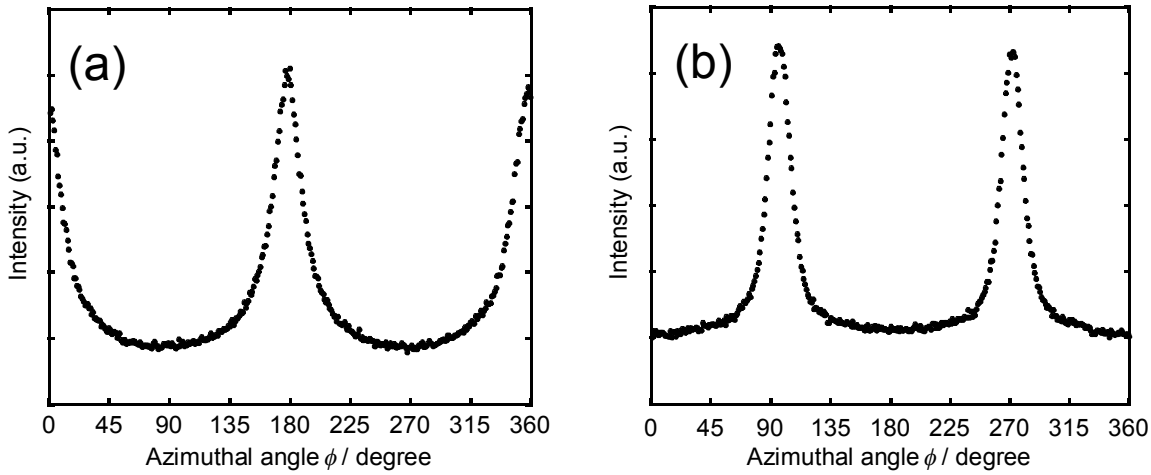

Figure 4-5. Azimuthal intensity scans of the (200) diffraction of CNCs: (a) data for CNC-2.0; (b) data for CNC-6.7. These two specimens are the same as those used in Figure 4-4.

There were several investigations into shear-induced orientation phenomena of CNCs in the aqueous suspensions put into a rotating cylinder[12,24,25]; the suspensions were all acidic, and, except for the Nishiyama's case, the CNC concentrations were constant during shear flow in the respective samples and mostly above the critical concentration for ordered mesophase formation (at rest). Ebeling et al. reported a two-step process on the shear alignment of cotton-derived CNCs (aspect ratio ≈ 10) in a 6.9 wt % aqueous suspension.[25] That is, at lower shear rates (< 5 s^{-1}), CNCs were aligned nearly at random in SD but showed a preferential orientation in the vertical direction (in the plane perpendicular to SD), whereas, at higher shear rates of ≥5 s^{-1}, CNCs were aligned individually parallel to SD. The estimation was based on small-angle X-ray scattering data obtained in two measuring setups, i) X-ray incidence being perpendicular to the surface of the sheared sample (normal view) and ii) that parallel to the flow direction SD (parallel or tangential view). They explained the result by assuming that CNCs formed anisotropic domains (i.e. mesophases) of uniplanar organization; the planar domains would orient along SD (each plane || SD) with the constituent CNCs distributed at random within the domains at low shear rates, before disruption at higher shear rates enabling the alignment of CNCs parallel to SD.

In the present chapter, the shear rates applied to CNC suspensions were >500 s^{-1} beyond 5 s^{-1} in any case of preparing CNC-2.0 and CNC-6.7 films. The *c*-axis orientation of CNCs to SD observed for CNC-6.7 is qualitatively consistent with the results of high-shear experiments reported by Ebeling et al.[25] and also by Orts et al.[24]; the latter group examined shear alignment of black spruce CNCs (aspect ratio, ca. 30–45) at suspension concentrations of 5–7 wt %. With regard to CNC-2.0, however, the alignment state of CNCs is completely different than the common pattern despite the application of a similar high-rate shear (580 s^{-1}), the longer axes of CNCs pointing to the transverse direction (TD) of the sheared sample. Accordingly, it is strongly suggested that the ionic atmosphere (which varies the critical CNC concentration of mesomorphic assembling) in the condensing suspensions would influence the CNC orientation in the films obtained under shear and drying.

A possible explanation for the present result is given in what follows. There will be two key points. One is basically correlated with the difference in ionic strength between Suspensions A and N. Suspension N (pH = 6.7) was prepared by neutralizing CNCs in the suspension equivalent to A (pH = 2.0) with NaOH aqueous solution. Therefore the counterions of the charged sulfate groups (OSO_3^-) on the surface of the CNCs in Suspension N are Na^+, being changed from H^+ that should be the counterions on the CNCs in Suspension A. Dong et al. studied effects of ionic strength and counterions on the isotropic–chiral nematic phase transition of CNC suspensions by using various electrolytes as additives.[4,26] The studies demonstrated that well-refined CNC suspensions only with H^+ counterions inherently associated with the surface sulfate groups formed an ordered phase at the lowest concentration of the used crystallites, and the added electrolytes generally suppressed anisotropic phase formation (i.e. increased the critical concentration of isotropic-mesophase transition) in any employment of acidic, neutral, or basic electrolytes. Accordingly, Suspension A would undergo the transition to form a chiral nematic phase at an appreciably lower concentration than Suspension N, in the process of water evaporation. This is supported by the SEM result (Fig. 4-3); the traces of chiral nematic-like organization were surely observed for the CNC-2.0 film. Then, the nematic layers emerging in Suspension A under drying should be deformed in the high-shear flow of >500 s^{-1}, differing from the situation at much lower shear rates in the Ebeling and coworkers' experiment[25]. In the present case using a rotated vessel, supposedly, the nematic layers might have wound and even rolled up so that the directors were oriented perpendicular rather than parallel to SD, as

illustrated in Figure 4-6a. In shear flow of pulp suspensions, similar behavior of rolling up or turning over of laterally assembled fibers has been experienced as a flocculation process.[27] By way of such a conversion of the arising ordered phase from a planar nematic into rolled form (resulting in a transversely extended body), the sheared suspension A would eventually transform into a solid film of CNC-2.0, in which the majority of CNCs are aligned in TD while the minor traces of chiral nematic arrangement still remain. In the other neutralized suspension N, most probably, the CNCs with sodium counterions hardly assumed a mesomorphic state; instead, the individual nano-rods could readily align along the shear flow at an earlier stage of the rotation process, and the uniaxial orientation distribution of CNCs with reference to SD would continue until gelation of the colloidal system toward the dry film of CNC-6.7 (see Fig. 4-6b).

In relation to the orientation of CNCs perpendicular to SD, it is known in suspension rheology that, when neutrally buoyant spheroids or rigid rods (treated as non-Brownian particles) are subjected to shear flow in viscous fluid media, they conditionally drift into a 'log-rolling' state with the longer axis oriented in the vorticity direction (TD in this chapter) via a complicate kayaking motion; this is concisely summarized, for example, in an article by Gunes et al.[28]. Typically, the log-rolling phenomenon has been detected by rheo-optical techniques for dilute or semi-dilute suspensions of short fibers with dimensions of >50 μm diameter and >1 μm length.[29,30] The applicability and contribution of such a log-rolling effect to the shear-induced orientation of CNC particles are undigested and unknown. The former orientation mechanism stated above is still hypothetical but offers a more convincing interpretation for the distinctive experimental result.

A serious question remains unresolved, however. It is the orientation pattern of CNC-6.7 (Fig. 4-6b), not of CNC-2.0 (Fig. 4-6a), that is in accordance with the earlier observation by Nishiyama et al.[12] for a shear-deformed CNC film. There was no sign of the CNC orientation to TD in their study. One factor in causing the result is the extremely high aspect ratio of the alga-derived CNC used there, the axial ratio being ~10 times larger than that of cotton-derived CNC. Plainly the former particles are much more advantageous to attainment of the uniaxial alignment along the shear flow. Another factor of great importance is the ionic strength of the CNC suspension employed in their experiment. Judging from the sampling procedure with no dialysis against water, the suspension was in a strongly acidic state (pH $\leq$ ~1) due to the excess remainder of the sulfuric acid used for

hydrolyzing cellulose fiber. This H^+-surplus condition should also suppress mesophase formation in the CNC suspension.[4] For these reasons, the sheared suspension would not undergo clear organization of nematic planar domains, and the development of CNC arrays to SD was smoothly realized in the dry film.

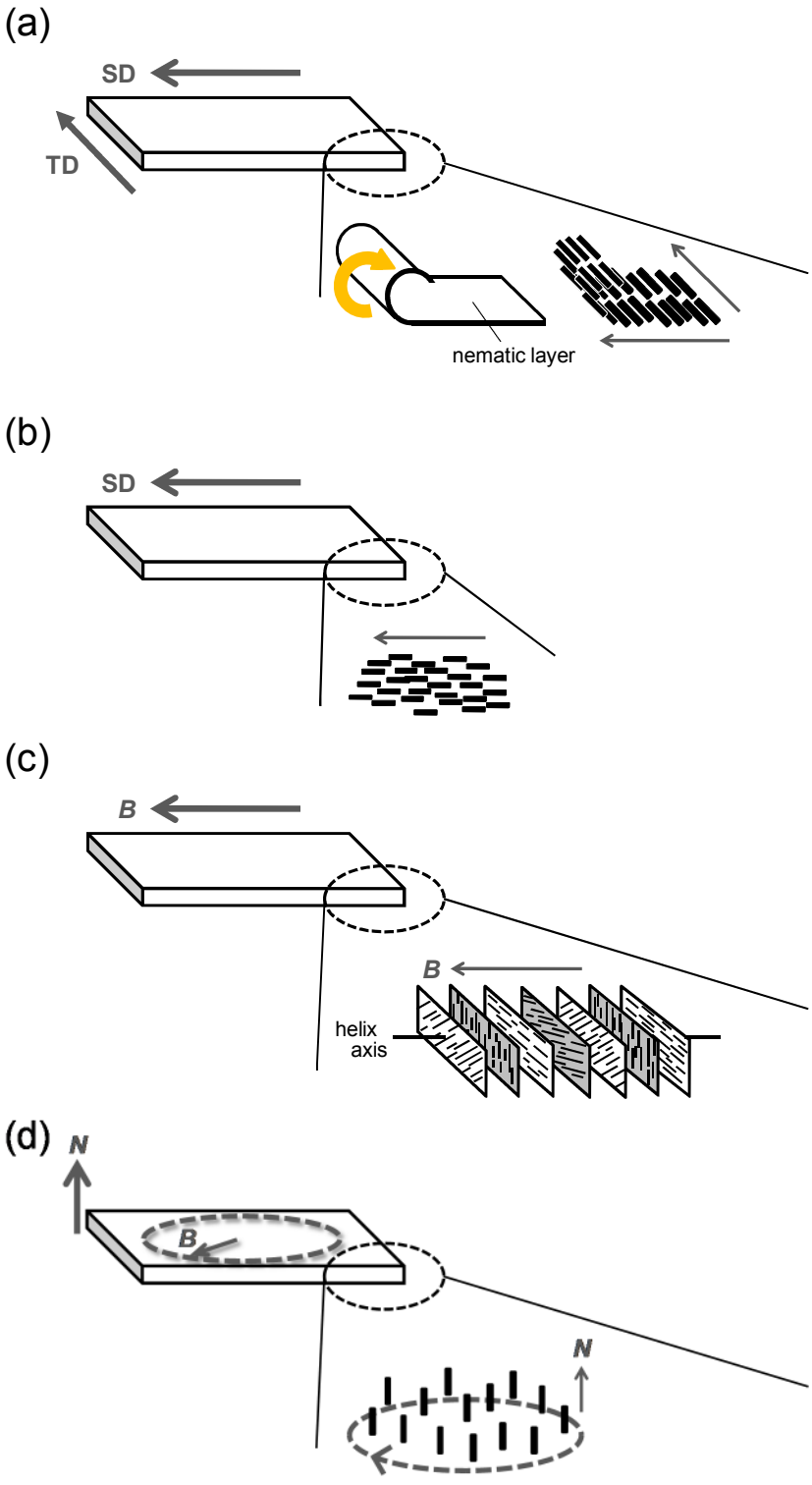

Figure 4-6. Different orientation patterns of CNC rods observed for shear-deformed CNC films, (a) CNC-2.0 and (b) CNC-6.7, and polymer composites, (c) PHEMA-CNC_{aniso}-s and (d) PHEMA-CNC_{aniso}-r.

4.3.3. Comparison of Orientation Development between Various Samples

To estimate the degree of CNC orientation for the present shear-deformed films, the orientation parameter f (= $(3\langle\cos^2\phi_c\rangle - 1)/2$) of the c-axis of CNC was quantified. In a similar way to that adopted in the previous chapter[18], the calculation was done by using the relation $f = -2f_a$ assuming a cylindrically symmetric distribution of CNC rods around TD (CNC-2.0) or SD (CNC-6.7); where f_a is the orientation parameter of the a-axis, which can be determined from the azimuthal data of the (200) diffraction intensity (Fig. 4-5). As a consequence, the authors obtained $f = 0.56$ for CNC-2.0 and $f = 0.68$ for CNC-6.7 (see upper two rows in Table 4-1), each data being an average with ±0.1 tolerance for three specimens belonging to the same sheared sample. The higher degree of orientation development in CNC-6.7 than in CNC-2.0 was in consistency with an FE-SEM observation indicating the distinction in orderliness of fibrillar alignment between the two samples.

As regards the case of CNC-6.7, the orientation parameter of ~0.7 is comparable with the one reported by Ebeling et al.[25] for a cotton-derived CNC suspension (6.9 wt %, see above); they determined $f \approx 0.75$ by small-angle X-ray scattering for the fluid under shear at a rate of 1700 s^{-1}. Meanwhile, Orts et al.[24] observed higher values of 0.8 or 0.9 as the order parameter of black spruce CNCs (axial ratio of 33 or 47) in the aqueous suspensions (5 or 7 wt % CNC) sheared at rates of ≥1000 s^{-1}, where the measurement was made by use of a small-angle neutron scattering technique. However, these data (ranging from ~0.7 to 0.9) of the orientation parameter are all lower than $f = 0.96$ obtained by Nishiyama et al.[12] for the shear-oriented film of green alga-derived CNC; probably, the primacy in orientation development of the latter would come from the extraordinarily high axial ratio of CNC, ~100.

Figure 4-6 also includes schematic illustrations of the orientation patterns of CNCs observed previously for PHEMA-CNC composites synthesized via magnetic field application to mesomorphic CNC suspensions;[18] two products were termed PHEMA-CNC_{aniso}-s (Fig. 4-6c) and PHEMA-CNC_{aniso}-r (Fig. 4-6d), according to whether the magnetic field (***B***) was static (s) or rotating (r). As shown in Table 4-1, the authors have obtained $f = 0.84$ (as to uniaxial alignment of the chiral nematic helical axis) for PHEMA-CNC_{aniso}-s and $f = 0.60$ (as to uniaxial alignment of the longer axis of CNC) for PHEMA-CNC_{aniso}-r; these are in a parallel or somewhat higher level, when compared with the data of $f \approx 0.6$–0.7 for the shear-oriented CNC films using the same cotton cellulose. For any of the four samples,

however, a passable level of orientation achievement may be admitted from a practical standpoint regarding the design of CNC-core polymer materials showing definite optical or mechanical anisotropy. The shearing method makes CNCs align to a certain degree with simpler equipment and procedure, while the non-contact technique using magnetic fields excels at aligning the fillers highly and uniformly.

Table 4-1. Evaluations of orientation parameters of the longitudinal axis of CNC for dry CNC films obtained under shear in different pH conditions and for PHEMA-CNC_{aniso} composites synthesized under different magnetic fields

Sample	Orientation parameter (*f*)	Reference axis of sample [b]
CNC-2.0	0.56 (avg.)	// TD
CNC-6.7	0.68 (avg.)	// SD
PHEMA-CNC_{aniso}-s	0.84 (helix axis) [a]; −0.42 (CNC axis) [a]	// ***B***
PHEMA-CNC_{aniso}-r	0.60 [a]	// ***N***

[a] Quoted from the previous chapter[18]

[b] See schematic illustrations in Fig. 4-6

References

(1) Marchessault, R. H.; Morehead, F. F.; Walter, N. M. *Nature* **1959**, *184*, 632–633.

(2) Revol, J. –F.; Bradford, H.; Giasson, J.; Marchessault, R. H.; Gray, D. G. *Int. J. Biol. Macromol.* **1992**, *14*, 170–172.

(3) Gray, D. G. *Carbohydr. Polym.* **1994**, *25*, 277–284.

(4) Dong, X. M.; Kimura, T.; Revol, J. –F.; Gray, D. G. *Langmuir* **1996**, *12*, 2076–2082.

(5) Dong, X. M.; Revol, J. –F.; Gray, D. G. *Cellulose* **1998**, *5*, 19–32.

(6) Habibi, Y.; Lucia, L. A.; Rojas, O. J. *Chem. Rev.* **2010**, *110*, 3479–3500.

(7) Klemm, D.; Kramer, F.; Moritz, S.; Lindström, T.; Ankerfors, M.; Gray, D. G.; Dorris, A. *Angew. Chem. Int. Ed.* **2011**, *50*, 5438–5466.

(8) Moon, R. J.; Martini, A.; Nairn, J.; Simonsen, J.; Youngblood, J. *Chem. Soc. Rev.* **2011**, *40*, 3941–3994.

(9) Dufresne, A. *Molecules* **2010**, *15*, 4111–4128.

(10) Eichhorn, S. J. *Soft Matter* **2011**, *7*, 303–315.

(11) Miao, C.; Hamad, W. Y. *Cellulose* **2013**, *20*, 2221–2262.

(12) Nishiyama, Y.; Kuga, S.; Wada, M.; Okano, T. *Macromolecules* **1997**, *30*, 6395–6397.

(13) Ureña-Benavides, E. E.; Brown, P. J.; Kitchens, C. L. *Langmuir* **2010**, *26*, 14263–14270.

(14) Uddin, A. J.; Araki, J.; Gotoh, Y. *Biomacromolecules* **2011**, *12*, 617–624.

(15) Gindle, W.; Keckes, J. *J. Appl. Polym. Sci.* **2007**, *103*, 2703–2708.

(16) Kvien, I.; Oksman, K. *Appl. Phys. A: Mater. Sci. Process.* **2007**, *87*, 641–643.

(17) Pullawan, T.; Wilkinson, A. N.; Eichhorn, S. J. *Biomacromolecules* **2012**, *13*, 2528–2536.

(18) Tatsumi, M.; Kimura, F.; Kimura, T.; Teramoto, Y.; Nishio, Y. *Biomacromolecules* **2014**, *15*, 4579–4589.

(19) Tatsumi, M.; Teramoto, Y.; Nishio, Y. *Biomacromolecules* **2012**, *13*, 1584–1591.

(20) Navard, P. *J. Polym. Sci., Part B: Polym. Phys.* **1987**, *25*, 1089–1098.

(21) Nishio, Y.; Yamane, T.; Takahashi, T. *J. Polym. Sci. Polym. Phys. Ed.* **1985**, *23*, 1053–1064.

(22) Majoinen, J.; Kontturi, E.; Ikkala, O.; Gray, D. G. *Cellulose* **2012**, *19*, 1599–1605.

(23) Sugiyama, J.; Vuong, R.; Chanzy, H. *Macromolecules* **1991**, *24*, 4168–4175.

(24) Orts, W. J.; Godbout, L.; Marchessault, R. H.; Revol, J. –F. *Macromolecules* **1998**, *31*, 5717–5725.

(25) Ebeling, T.; Paillet, R.; Borsali, R.; Diat, O.; Dufresne, A.; Cavaillé, J. –Y.; Chanzy, H. *Langmuir* **1999**, *15*, 6123–6126.

(26) Dong, X. M.; Gray, D. G. *Langmuir* **1997**, *13*, 2404–2409.

(27) Chen, B.; Tatsumi, D.; Matsumoto, T. *Sen'i Gakkaishi* **2003**, *59*, 471–478.

(28) Gunes, D.Z.; Scirocco, R.; Mewis, J.; Vermant, J. *J. Non-Newtonian Fluid Mech.* **2008**, *155*, 39–50.

(29) Bartram, E.; Goldsmith, H. L.; Mason, S. G. *Rheol. Acta.* **1975**, *14*, 776–782.

(30) Iso, Y.; Koch, D. L.; Cohen, C. *J. Non-Newtonian Fluid Mech.* **1996**, *62*, 115–134.

Chapter 5
Summary and Conclusions

A sequence of studies in the present thesis was carried out to exemplify the designing and fabrication of novel cellulose-polymer composites that display high thermomechanical performance and optical functionality, mainly derived from the mesomorphic characteristics of cellulose nanocrystals (CNCs) and, more practically, to enhance the availability of CNCs as nano- or meso-fillers. The major results are briefly listed below:

1. Locking-in of the mesomorphic assembly of CNC suspensions into polymer solids was successfully accomplished. Transparent and, more or less, birefringent composites of poly(2-hydroxyethyl methacrylate) (PHEMA)-CNC were obtained. The CNC incorporations into the PHEMA matrix improved the original thermal and mechanical properties of the vinyl polymer material (Chapter 2).

2. Polymer composites PHEMA-CNCs reinforced with specifically oriented CNCs were synthesized from the colloidal suspensions exposed to a strong magnetic field. CNCs were aligned in the composites distinctively according to the sort of the pre-applied magnetic field, when the anisotropic phases of the suspensions were used for the preparation. The observed coherent response of CNCs forming the mesomorphic assembly is of great significance in the magnetic orientation behavior of CNC suspensions. The fixed CNC's orientation states reflected the definite mechanical anisotropy of the composites (Chapter 3).

3. Oriented cellulose films were made from CNC aqueous suspensions under shear flow. The obtained films were optically birefringent and composed of fine fibrillar structures aligned mostly in good order. The orientation pattern of CNCs in the films was affected by the ionic condition of the sheared suspension (Chapter 4).

More specific results obtained in the individual chapters of this thesis are summarized as follows.

Chapter 2.

PHEMA-CNC composites were successfully synthesized from suspensions of CNC (acid-treated cotton microfibril) in an aqueous HEMA solution, via polymerization of the vinyl monomer in the mixed solvent. Three aliquots differently fractionated from a CNC/water/HEMA suspension (5.0 wt % CNC; water /HEMA = 0.46–1.1 : 1 in weight) were separately converted into a film of composite, which was termed PHEMA-CNC_{aniso}, PHEMA-CNC_{iso}, or PHEMA-CNC_{mix} according to the difference in the state of phase-equilibrium between the aliquots: the isotropic phase, anisotropic phase, and embryonic non-separating mixture.

All the composites were transparent and, more or less, birefringent. Even though the polymerization process was accompanied by condensation of the dispersoid CNC due to evaporation of water, POM observations readily distinguished the difference in the development stage of mesoscopic ordering between the three composite products. A fingerprint texture characteristic of chiral nematic (cholesteric) liquid crystals prevailed widely in PHEMA-CNC_{aniso}, but rather locally appeared in PHEMA-CNC_{iso}. PHEMA-CNC_{mix} was wholly poor in such a liquid-crystalline organization. FE-SEM investigation for PHEMA-CNC_{aniso} revealed that many fibrous entities of CNC were aligned with their respective longer axes rotating helically to make a chiral nematic arrangement in the polymer matrix.

The incorporation of CNC fillers into the composites at <10 wt % resulted in only a small elevation in T_g of the vinyl polymer. For any of the three composites, however, it was shown by DMA measurements that the locking-in of the respective CNC assemblies led to an increase in the glassy modulus E' of PHEMA and to a marked suppression of the E'-drop at temperatures higher than T_g (~110 °C) of the polymer. This demonstrates a reinforcement effect of the CNC dispersions exerted on the polymer matrix to improve the thermomechanical property. It was also found as a secondary effect that the modulus E' of the respective composites reincreased with temperature in a range of 150–190 °C, which was due to cross-linking of PHEMA molecules following a dehydration reaction catalyzed by the acidic CNC filler. This cross-linking would be used as a post-treatment to invest the inherently hydrophilic polymer material with moderate hydrophobicity as well as thermal stability.

In a tensile mechanical test, all the composites exhibited a harder elasticity against extension of film specimens, compared with CNC-free PHEMA. Especially PHEMA-CNC_{aniso} surpassed the other composites and PHEMA in the performance of stiffness and strength. It should be noted, however, that even the composite PHEMA-CNC_{aniso} is mechanically isotropic (when viewed as a macroscopic material) because the optically birefringent domains of CNC are spread at random therein.

Chapter 3.

Polymer composites reinforced with specifically oriented CNCs were prepared. The composites of PHEMA-CNC were synthesized from suspensions of cotton-derived CNC in an aqueous HEMA solution, via application of a strong magnetic field (8 T) and polymerization of the vinyl monomer in the solvent. Isotropic and anisotropic phases fractionated from CNC/water/HEMA suspensions (~6.0 wt % CNC; water/HEMA = 0.56 : 1 in weight) were each exposed to various magnetic fields of static (s), rotational (r), and elliptical (e) types. The resulting respective orientation states of dispersed CNCs were immobilized into the corresponding polymer composites by UV-induced polymerization of HEMA. The composite products were named PHEMA-CNC_{iso}-s, PHEMA-CNC_{aniso}-s, PHEMA-CNC_{iso}-r, etc.

In PHEMA-CNC_{aniso}-s, a fingerprint texture characteristic of chiral nematic liquid crystals developed with straight retardation lines running entirely parallel. In contrast, no fingerprinted structure appeared in PHEMA-CNC_{aniso}-r, which demonstrates that the mesoscopic assembly in the fractionated suspension converted from the original chiral nematic into unidirectional nematic state and this was further carried over into the polymer composite. FE-SEM measurements revealed numerous fibrous entities (assimilation of CNCs) oriented to almost one direction in PHEMA-CNC_{aniso}-r, which also confirmed the uniform array of fingerprints in PHEMA-CNC_{aniso}-s. More decisively, WAXD analyses showed that the helix axis of the uniform chiral nematic domain present in PHEMA-CNC_{aniso}-s was oriented parallel (therefore CNC rods lying perpendicular) to the field vector, while the longitudinal axis of CNCs in PHEMA-CNC_{aniso}-r was aligned in good order perpendicular to the plane of rotating magnetic field. Meanwhile, in PHEMA-CNC_{iso}-s and PHEMA-CNC_{iso}-r derived from isotropic CNC suspensions, the

particles were distributed at nearly random, and the magnetic alignment of them was substantially unattainable therein. The PHEMA-CNC_{aniso}-e series was prepared under various conditions of modulating the field rotation, but a similar orientation pattern to that in PHEMA-CNC_{aniso}-r prevailed therein with no preferential orientation of the shorter axes around the longitudinal axis of CNC. This result may be ascribable principally to the intrinsic anisotropy in the magnetic susceptibility (χ) of CNC, as suggested by a formulation of $|\chi_1| \approx |\chi_2| << |\chi_3|$.

DMA measurements confirmed that the CNC dispersions exerted a reinforcing effect on the polymer matrix so as to improve the thermomechanical property, in common. In addition, the present DMA study disclosed the mechanical anisotropy that reflects the CNC's orientational states in the matrix, most explicitly for PHEMA-CNC_{aniso}-s and PHEMA-CNC_{aniso}-r. In comparison, PHEMA-CNC_{aniso}-r exhibited the highest modulus in the direction privileged by the alignment of CNC rods, entirely over the temperature range of ≤200 °C. The authors thus successfully demonstrated an anisotropy and ensuing improvement in the thermomechanical performance of PHEMA-CNC composites by means of the magnetic orientation of CNC assemblage in the process of synthesis. This would be of great significance in polymer material designs using CNCs as reinforcers.

Chapter 4.

Oriented films of cotton-derived CNC (axial ratio, ~10) were prepared from aqueous suspensions (3–4 wt % CNC) under high-rate shear (>500 s^{-1}) accompanied by water evaporation. The film products were named CNC-2.0 and CNC-6.7 according as the starting suspension was in an acidic (pH = 2.0) or neutral (pH = 6.7) condition; the neutral suspension (N) was made by addition of NaOH into the parent suspension (A) of pH = 2.0. Comparative characterization of the oriented CNC films was performed by POM and FE-SEM microscopy and WAXD measurements.

The films were optically birefringent and composed of fine fibrillar structures aligned mostly in good order; the running way of the fibrous entities was, in perspective, parallel to the shear direction (SD) in CNC-6.7, but perpendicular to SD in CNC-2.0. In correspondence with the microscopic observations, WAXD analysis revealed that the longitudinal axes of CNCs were aligned preferentially perpendicular to SD in CNC-2.0 and

parallel to SD in CNC-6.7. In the drying process of the sheared suspensions A and N, probably, the formation of (chiral) nematic ordered phase occurred in A, but scarcely did in N, which stands on the difference in the counterions of surface-sulfated CNCs between the two (H^+ in A and Na^+ in N). This deduction was also supported by FE-SEM observations of surface morphology for the corresponding two dry films. In the suspension N free of mesomorphic structuring, therefore, CNC particles were allowed to individually align parallel to SD so as to produce the common uniaxial orientation in the CNC-6.7 film. With regard to the suspension A under a rotatory shear flow, it was assumed that the nematic planar domains arriving with time were deformed by winding-up force so that the nematic directors were arranged perpendicular to SD, which gave rise to the transverse orientation pattern of the elemental CNC rods in the CNC-2.0 film.

The degree of orientation development ($f \approx 0.6$–0.7) in the two CNC films was taken to be in a parallel or somewhat lower level, in comparison with the orientation achievement of the same cotton CNC in the polymer composites (PHEMA-CNC_{aniso}-s and PHEMA-CNC_{aniso}-r) that were synthesized under a static or rotational magnetic field in chapter 3. However, the success in controlling the CNC orientation with the ionic condition of the sheared suspension is of great significance, from both scientific and practical points of view.

Looking over the results summarized above, the author would like to give the following concluding remarks: The rod-shaped fragments of crystalline microfibril, CNCs, can work for sure as a stiff nano-filler to effectively reinforce bulk matrices of other polymers. Furthermore, CNCs in liquid-crystalline suspensions are able to behave in an ordered assemblage under external force fields such as shear-flow and magnetic fields, and the externally controlled orientation states of CNCs (and, of course, the self-organized chiral nematic architecture of CNCs as well) can be carried over into solid materials including composites with other polymer (or even inorganic) components. In view of these, the use of CNCs as "meso-fillers" as well as nano-fillers is quite promising and will expand the opportunities to design advanced cellulosic materials. The author expects related research fields to be further vitalized in the future decade, and also hopes that the present work may be partly contributable to the activation.

List of Publications

The contents of this thesis have been described in the following publications.

Original Papers

1. "Polymer Composites Reinforced by Locking-In a Liquid-Crystalline Assembly of Cellulose Nanocrystallites", Mio Tatsumi, Yoshikuni Teramoto, and Yoshiyuki Nishio, *Biomacromolecules* **2012**, 13, 1584–1591. **(Chapter 2)**
2. "Anisotropic Polymer Composites Synthesized by Immobilizing Cellulose Nanocrystal Suspensions Specifically Oriented under Magnetic Fields", Mio Tatsumi, Fumiko Kimura, Tsunehisa Kimura, Yoshikuni Teramoto, and Yoshiyuki Nishio, *Biomacromolecules* **2014**, 15, 4579–4589. **(Chapter 3)**
3. "Different Orientation Patterns of Cellulose Nanocrystal Films Prepared from Aqueous Suspensions by Shearing under Evaporation", Mio Tatsumi, Yoshikuni Teramoto, and Yoshiyuki Nishio, to be published, *Cellulose*. **(Chapter 4)**

Commentary (Book Chapter)

1. Yoshiyuki Nishio, Mio Tatsumi, and Junichi Sato: "Liquid Crystals of Cellulose and Derivatives" In "Handbook for New Functional Developments of Glyco-materials" (K. Akiyoshi et. al., eds), NTS Pub., Tokyo, Part7, Chap. 2, Sect. 7, to be published (in Japanese).

International Conference

1. "Anisotropic Polymer Composites Reinforced with Various Assemblies of Cellulose Nanicrystallites: Orientation-Controlled Synthesis under Magnetic Field", Mio Tatsumi, Fumiko Kimura, Tsunehisa Kimura, Yoshikuni Teramoto, and Yoshiyuki Nishio, *The 3rd International Cellulose Conference*, Sapporo, Japan, October, 2012.

Acknowledgements

The present thesis is based on the studies which the author has carried out in Laboratory of Chemistry of Composite Materials, Division of Forest and Biomaterials Science, Graduate School of Agriculture, Kyoto University, from 2008 to 2015, under the guidance of Professor Dr. Yoshiyuki NISHIO.

First of all, the author would like to express her sincerest gratitude to Professor Dr. Yoshiyuki NISHIO, Laboratory of Chemistry of Composite Materials, Division of Forest and Biomaterials Science, Graduate School of Agriculture, Kyoto University, for his continuous guidance, invaluable suggestions and assistance, and kindest encouragement during the entire course of this work. A sequence of studies in the present thesis would not have been possible to accomplish without his warmest and kindest acceptance as a doctoral student.

The author is deeply grateful to Professor Dr. Tsunehisa KIMURA, Laboratory of Fibrous Biomaterials, Division of Forest and Biomaterials Science, Graduate School of Agriculture, Kyoto University, and Professor Dr. Toshiyuki TAKANO, Laboratory of the Chemistry of Biomaterials, Division of Forest and Biomaterials Science, Graduate School of Agriculture, Kyoto University, for their critical readings of the manuscript and valuable suggestions.

The author wishes to express her gratitude to Associate Professor Dr. Yoshikuni TERAMOTO, Department of Applied Life Science, Faculty of Applied Biological Science, Gifu University, for his helpful suggestions and comments.

The author acknowledges Professor Dr. Tsunehisa KIMURA, Laboratory of Fibrous Biomaterials, Division of Forest and Biomaterials Science, Graduate School of Agriculture, Kyoto University, and Research Associate Dr. Fumiko KIMURA, Laboratory of Fibrous Biomaterials, Division of Forest and Biomaterials Science, Graduate School of Agriculture, Kyoto University, for having afforded the experimental equipment of strong magnetic fields and measurement facilities of WAXD, and for their kind instruction and advice.

The author acknowledges Professor Dr. Keiji TAKABE, Laboratory of Tree Cell Biology, Division of Forest and Biomaterials Science, Graduate School of Agriculture, Kyoto University, for having afforded the measurement facilities of TEM and the microtome.

The author acknowledges Lecturer Dr. Mariko AGO, Department of Nano Material and Bio Engineering, Faculty of Science and Engineering, Tokushima Bunri University, for having afforded the measurement facilities of FE-SEM.

The author acknowledges Professor Emeritus Takayoshi MATSUMOTO, Division of Forest and Biomaterials Science, Graduate School of Agriculture, Kyoto University, for his warm encouragement.

The author acknowledges Lecturer Dr. Mariko YOSHIOKA, Laboratory of Chemistry of Composite Materials, Division of Forest and Biomaterials Science, Graduate School of Agriculture, Kyoto University, for her kind cooperation.

The author wishes to thank her colleagues in the Laboratory of Chemistry of Composite Materials, Division of Forest and Biomaterials Science, Graduate School of Agriculture, Kyoto University, for their kind help in many ways.

Last not least, the author's special appreciation goes to her whole family; my parents Kakurou OKAZAKI and Michiko OKAZAKI, Hajime TATSUMI and Setsuko TATSUMI, my sisters Nao OKAZAKI and Saori OKAZAKI, my brother Hirosuke TATSUMI, my delightful husband Daisuke TATSUMI, and my cheerful daughter Mani TATSUMI, for their understanding, and warmest support and continuous encouragement.

May 2015

Mio TATSUMI